Title

Cross-species functional diversity within the PIN auxin efflux protein family

Authors

Devin Lee O'Connor[1,^], Samuel Elton[1*], Fabrizio Ticchiarelli[1*], Mon Mandy Hsia[2], John Vogel[3,4], Ottoline Leyser[1].

Affiliations

[1]Sainsbury Laboratory University of Cambridge, Cambridge, UK.

[2]USDA-ARS Western Regional Research Center, Albany, CA.

[3]U.S. Department of Energy Joint Genome Institute, Walnut Creek, CA.

[4]Department of Plant and Microbial Biology, University of California, Berkeley, CA.

*These authors contributed equally.

^Author for Correspondence: Devin Lee O'Connor devin.oconnor@slcu.cam.ac.uk

Abstract

In Arabidopsis, development during flowering is coordinated by transport of the hormone auxin mediated by polar-localized PIN-FORMED1 (AtPIN1). However, Arabidopsis has lost a PIN clade sister to AtPIN1, Sister-of-PIN1 (SoPIN1), which is conserved in flowering plants. We previously proposed that the AtPIN1 organ initiation and vein patterning functions are split between the SoPIN1 and PIN1 clades in grasses. Here we show that in the grass Brachypodium *sopin1* mutants have organ initiation defects similar to Arabidopsis *atpin1*, while loss of *PIN1* function in Brachypodium has little effect on organ initiation but alters stem growth. Heterologous expression of Brachypodium SoPIN1 and PIN1b in Arabidopsis provides further evidence of functional specificity. SoPIN1 but not PIN1b can mediate flower formation in null *atpin1* mutants, although both can complement a missense allele. The behavior of SoPIN1 and PIN1b in Arabidopsis illustrates how membrane and tissue-level accumulation, transport activity, and interaction contribute to PIN functional specificity.

Introduction

The plant hormone auxin is an essential mobile signal controlling growth and patterning throughout plant development (Leyser, 2010). Auxin can passively enter cells, triggering a vast array of downstream signaling events (Wang and Estelle, 2014), but it cannot easily exit the cell without active transport (Raven, 1975; Rubery and Sheldrake, 1974). As a result, directional efflux mediated by the polar-localized PIN-FORMED (PIN) efflux carriers can organize auxin flows and accumulation patterns, creating concentration maxima and paths of transport that regulate growth, position organs, and pattern tissues

(Adamowski and Friml, 2015). Because auxin itself feeds back to regulate PIN-mediated transport both transcriptionally and post-transcriptionally (Leyser, 2006), the transport system shows remarkable robustness and plasticity. For example, compensatory changes in PIN abundance between PIN family members can mitigate PIN loss-of-function mutant phenotypes (Blilou et al., 2005; Paponov et al., 2005; Vieten et al., 2005), environmental inputs can trigger tissue-level changes in PIN abundance and polarity leading to altered plant growth (Habets and Offringa, 2014), and auxin transport paths can be reorganized in response to injury (Sauer et al., 2006; Xu et al., 2006), or spontaneously in tissue culture (Gordon et al., 2007). The self-organizing properties of the auxin transport system thus gives this patterning mechanism extraordinary versatility, and allows it to coordinate both local and long-range communication in plants.

The correct initiation and positioning of organs (leaves, flowers, stems) in the growing tip, or shoot apical meristem, of *Arabidopsis thaliana* (Arabidopsis) plants requires the action of the PIN-FORMED1 (AtPIN1) auxin efflux carrier (Okada et al., 1991). AtPIN1 is targeted to the plasma membrane and polarized in cells (Gälweiler et al., 1998). In the meristem epidermis, polarization of AtPIN1 in neighboring cells converges around the initiation sites of new organs, suggesting that polarized AtPIN1 concentrates auxin into local maxima causing organ initiation (Benková et al., 2003; Heisler et al., 2005; Reinhardt et al., 2003). Accordingly, in *atpin1* loss-of-function mutants, or if auxin transport is pharmacologically inhibited, organ initiation is aborted, but it can be rescued with local auxin application to the meristem flank (Reinhardt et al., 2003; Reinhardt et al., 2000). Organ initiation in *atpin1* mutants can also be rescued with epidermal-specific

AtPIN1 expression (Bilsborough et al., 2011), and reducing AtPIN1 function specifically in the epidermis compromises organ positioning and initiation (Kierzkowski et al., 2013), demonstrating the importance of convergent AtPIN1 polarization in the epidermis during organ formation.

The recurrent formation of AtPIN1 convergence points surrounding auxin maxima in the meristem epidermis has been the focus of several computational models that attempt to explain how auxin feeds back on its own transport via AtPIN1 to concentrate auxin and control organ spacing (Abley et al., 2016; Bayer et al., 2009; Bhatia et al., 2016; Heisler et al., 2010; Jönsson et al., 2006; Smith et al., 2006; Stoma et al., 2008). However, AtPIN1 is also expressed during the patterning of the vascular strands formed coincident with organ positioning, and in these sub-epidermal cells AtPIN1 is polarized rootward, away from the presumed auxin maxima, suggesting that AtPIN1 polarity with respect to auxin concentration may vary across tissues or over developmental time (Bayer et al., 2009).

Indeed, AtPIN1 has several functions post organ initiation that are not necessarily associated with convergent polarization patterns (Gälweiler et al., 1998; Scarpella et al., 2006). AtPIN1 is not required for organ formation during the vegetative phase. Mutants lacking AtPIN1 form leaves, but they are misplaced and have severe morphological and vascular defects similar to those observed upon pharmacological inhibition of auxin transport, suggesting an important role for AtPIN1 in post-initiation morphogenesis and vein patterning in leaves (Guenot et al., 2012; Sawchuk et al., 2013; Verna et al., 2015). Furthermore, in mature tissues, AtPIN1 is polarized rootward in vascular-associated cells and is required for efficient long distance transport of auxin down the shoot in the

polar auxin transport stream, and this has been proposed to play an important role in the regulation of shoot branching (Bennett et al., 2016; Bennett et al., 2006; Gälweiler et al., 1998; Shinohara et al., 2013). Mutations in other PIN family members in combination with *atpin1* mutants suggest further functions in embryo development, root development and during plant growth responses to light and gravity (Leyser, 2005). Unfortunately, the myriad roles for AtPIN1 during inflorescence development are genetically obscured by the severity of *atpin1* organ initiation defects.

We previously showed that all sampled flowering plants outside of the Brassicacea family have a clade of PIN proteins phylogenetically sister to the PIN1 clade (The Sister-of-PIN1 or SoPIN1 clade), while Arabidopsis and other Brassicacea species have lost this clade (O'Connor et al., 2014). During organ initiation in the grass *Brachypodium distachyon* (Brachypodium) which has both PIN1 and SoPIN1 clades, SoPIN1 is highly expressed in the epidermis, polarizes towards presumed auxin maxima, and forms convergent polarization patterns during the formation of new organs, suggesting a role in creating the auxin maxima required for organ initiation. In contrast, the duplicate Brachypodium PIN1 clade members, PIN1a and PIN1b, are not highly expressed in the epidermis, orient away from presumed auxin maxima, and are primarily expressed during patterning in the sub-epidermal tissues. Thus, the combined expression domains and polarization behaviors of SoPIN1, PIN1a, and PIN1b in Brachypodium largely recapitulate those observed for AtPIN1 alone in Arabidopsis.

The dynamic localization and polarization patterns of the Brachypodium SoPIN1 and PIN1 clades can be modeled with two different polarization modes with respect to auxin. PIN behaviors can be captured by a model in which SoPIN1 polarizes “up-the-gradient”,

towards the neighboring cell with the highest auxin concentration, while PIN1a and PIN1b polarize “with-the-flux”, accumulating in the membrane with the highest net auxin efflux (O'Connor et al., 2014). Both polarization modes were previously applied to AtPIN1 in order to capture the switch in polarity observed during organ initiation and vein patterning, first orienting toward the auxin maximum during convergence point formation, then orienting away from the maximum below the epidermis during vein patterning (Bayer et al., 2009). These localization and modeling results suggest that in most angiosperm species the organ placement and vascular patterning functions attributed to AtPIN1 in Arabidopsis are split between the PIN1 and SoPIN1 clades, and that these two clades have different polarization properties with respect to auxin.

Exploring this hypothesis, here we present the functional analysis of both the SoPIN1 and PIN1 protein clades in Brachypodium, a species with the canonical two-clade family structure. We show that SoPIN1 and the PIN1 clade members PIN1a and PIN1b have different functions during Brachypodium development, with SoPIN1 being required for organ initiation during the flowering phase, and PIN1a and PIN1b regulating stem growth. Using heterologous expression in Arabidopsis, we show that the SoPIN1 and PIN1b proteins have different accumulation, polarization, and transport behaviors that result in different functional properties independent of transcriptional context. In addition to elucidating several ways in which PIN family members can be functionally distinct, these results suggest that the Arabidopsis AtPIN1 protein represents an example of an evolutionary phenomenon the opposite of subfunctionalisation in which protein functions are amalgamated into a single protein rather than diversified amongst paralogs. AtPIN1

has a repertoire of roles, and associated polarization behaviors that are distributed among several clades of PIN proteins in most flowering plants.

Results

The SoPIN1 and PIN1 clades have different functions in Brachypodium

We targeted Brachypodium SoPIN1, PIN1a, and PIN1b with gene-specific Clustered Regularly Interspaced Short Palindromic Repeats (CRISPR) and for all three genes recovered independent single base-pair lesions causing frame shifts and premature stop codons (Figure 1A). The wild-type Brachypodium inflorescence meristem normally makes several lateral spikelet meristems (lsm), before producing a terminal spikelet meristem (tsm) (Figure 1B)(Derbyshire and Byrne, 2013). Both lateral and terminal spikelet meristems are consumed in the production of florets (Figure 1D, 1F). The *sopin1-1* inflorescence meristems had severe organ and spikelet branch initiation defects (Figure 1C), which resulted in reduced total whole-plant spikelet number (Figure 1H). When spikelets did form, *sopin1-1* spikelet meristems were often devoid of new organs (Figure 1E), and very few recognizable florets were produced (Figure 1I). In support of the *sopin1-1* lesion being responsible for these varied inflorescence phenotypes, we complemented inflorescence development and seed set by crossing *sopin1-1* to the previously published SoPIN1-CITRINE fusion line (Figure 1 – supplement 1)(O'Connor et al., 2014). The pleotropic defects displayed by *sopin1-1* in

the inflorescence are remarkably similar to loss-of-function *pin1* mutants in *Arabidopsis* (Okada et al., 1991) and *Cardamine hirsuta* (Barkoulas et al., 2008).

In wild-type spikelet meristems, SoPIN1 convergence point formation is coincident with an increase in the auxin signaling reporter DR5 (O'Connor et al., 2014), as well as a decrease in the nuclear auxin response reporter protein DII-Venus (Brunoud et al., 2012) (DII) (Figure 1J), which functions in Brachypodium and is degraded in the presence of auxin in spikelet meristems (Figure 1 - supplement 2). In *sopin1-1* meristems, DII accumulation was uniformly high for long stretches of the epidermis, and the patterned reduction of DII both in the meristem epidermis and internally failed to occur, suggesting a failure to organize auxin maxima (Figure 1K arrow).

In contrast to the severe defects of *sopin1-1*, organ initiation in *pin1a-1* and *pin1b-1* single mutants was largely unaffected. The mature inflorescences of both *pin1a-1* and *pin1b-1* had normal spikelets (Figure 1F), and spikelet meristem morphology was indistinguishable from wild-type (Figure 1G). Mutant *pin1a-1* plants appeared visually wild-type, but we measured a slight increase in total spikelet number (Figure 1H). Mutant *pin1b-1* plants were similar to wild-type with respect to both spikelet and floret numbers (Figure 1H, 1I), but often had bent apical internodes (Figure 1F arrowhead). While *pin1a-1* and *pin1b-1* single mutants had no clear organ initiation defects they showed changes in internode length (Figure 2). Plant stature in *pin1a-1* mutants was largely indistinguishable from wild-type (Figure 2B), but we measured a small reduction in the length of the I4 internode (Figure 2E). In contrast, *pin1b-1* plants were easily distinguished from wild-type because of a significant increase in internode length at the base of the plant, resulting in greater overall plant height (Figure 2E). The elongated

basal internodes and bent stems of *pin1b-1* resulted in a less compact plant architecture compared to the other genotypes (Figure 2C). The increase in basal internode length in *pin1b-1* single mutants was rescued by the previously published PIN1b-CITRINE florescent reporter (O'Connor et al., 2014) (Figure 2 – supplement 1).

The PIN1a and PIN1b duplication is specific to, but conserved within the grasses (O'Connor et al., 2014). Thus, we suspected these two genes would show a degree of genetic redundancy. Indeed, *pin1a-1/pin1b-1* (*pin1a/b*) double mutants showed a synergistic phenotype, with severely reduced plant height (Figure 2D), resulting primarily from reduced internode growth in the upper internodes (Figure 2E). However, despite loss of both PIN1a and PIN1b function, *pin1a/b* double mutants made normal spikelet meristems (Figure 1G), had a wild-type total spikelet number (Figure 1H), and showed only a small reduction in floret number in the terminal spikelet (Figure 1I). In addition, unlike *sopin1-1* plants, *pin1a/b* double mutants set ample seed.

Combined these phenotypes provide further support for functional distinction between the SoPIN1 and PIN1 clades, and indicate that while the PIN1 clade is expendable for organ initiation in Brachypodium, it is involved in the regulation of internode growth.

AtPIN1, SoPIN1, and PIN1b accumulate differently in Arabidopsis under the same transcriptional control

During organ formation in the Brachypodium shoot, expression of both SoPIN1 and PIN1b precedes PIN1a, which only accumulates significantly at the sites of vein

formation after the organs begin to grow (O'Connor et al., 2014). In the earliest stages of initiation, prior to the periclinal cell divisions that are the hallmark of morphogenesis, SoPIN1 forms convergent polarization patterns around the presumed auxin maxima in the meristem epidermis, while PIN1b is expressed internally and orients away from the maxima (O'Connor et al., 2014). Because of their early expression, opposing polarization patterns, and their clear single-mutant phenotypes in Brachypodium, we focused on characterizing SoPIN1 and PIN1b as representatives of the SoPIN1 and PIN1 clades.

The difference between the *sopin1-1* and *pin1b-1* phenotypes in Brachypodium could be due to their different expression patterns and not necessarily to differences in their polarization with respect to auxin concentration or flux as previously hypothesized (O'Connor et al., 2014). In order to assess the functional differences between the proteins, independent of transcriptional context, we expressed both Brachypodium proteins tagged with CITRINE (a YFP derivative) in wild-type Arabidopsis (Columbia, Col-0) under the control of a 3.5kb Arabidopsis *PIN1* promoter fragment which includes sequences known to drive PIN1 expression sufficient to complement *pin1* mutants (*proAtPIN1*) (Benková et al., 2003; Heisler et al., 2005). In the Arabidopsis inflorescence meristem, wild-type AtPIN1 forms convergent polarization patterns that mark the sites of initiating flower primordia (Figure 3A). Remarkably, despite the loss of the SoPIN1 clade from Arabidopsis, Brachypodium SoPIN1 also created clear convergent polarization patterns in Arabidopsis inflorescence meristems but was less abundant in the central domain of the apical dome (Figure 3B, 25 of 27 meristems from 4 independent transgenic events). Similar to AtPIN1, SoPIN1 protein abundance was highest in the

meristem epidermis, and SoPIN1 convergence points were most clearly observed surrounding I2 and I1 primordia (Figure 3B). Below the epidermis wild-type AtPIN1 accumulates in small groups of cells that will become the vasculature (Figure 3 – supplement 1 panel A arrows). In contrast, sub-epidermal SoPIN1 accumulated in an ill-defined ring shape surrounding the meristem central domain without distinct foci of expression (Figure 3 – supplement 1 panel B, 15 of 23 meristems from 4 independent transgenic events).

In contrast to both AtPIN1 and SoPIN1, under the same promoter significant PIN1b accumulation was absent from the meristem epidermis in 19 of 29 meristems from 7 independent transgenic events. In the few meristems where PIN1b accumulated in the epidermis, it did not show clear convergent polarization patterns, and its polarity was often unclear (Figure 3C). Within initiating organs, PIN1b often localized to punctate vesicular bodies inside cells, not in the cell membrane (Figure 3C arrowhead). PIN1b accumulation remained low just below the meristem apex, but in contrast to SoPIN1, PIN1b formed defined domains around the presumptive developing vascular bundles similar to AtPIN1 (Figure 3 – supplement 1 panel C arrows). The lack of PIN1b protein in the meristem epidermis was not due to silencing of the transgene in these lines because we observed abundant PIN1b protein in the developing vasculature below the apex, even in plants where the meristem had no detectable epidermal expression (Figure 3F) (8 samples from 4 events). In contrast, AtPIN1 and SoPIN1 accumulated in both the vasculature and the epidermis in these more mature tissues (Figure 3D, 3E), although SoPIN1 seemed more abundant in the epidermis than AtPIN1 (see arrows) (SoPIN1 - 5 samples from 2 events).

In order to determine whether there were similar tissue-level differences in protein accumulation in mature tissues, where AtPIN1 is implicated in branch control, we imaged AtPIN1, SoPIN1, and PIN1b in the basal internode in mature plants 1cm above the rosette. Here, AtPIN1 normally accumulates in a highly polar manner in the rootward plasma membranes of cambium (ca) and xylem parenchyma (xp) vascular-associated tissues (Figure 3G, 3J) (Bennett et al., 2016; Gälweiler et al., 1998). Here PIN1b accumulated in a similar pattern to AtPIN1 (Figure 3I, 3L. 10 samples from 5 events). In contrast, in addition to accumulating in the cambium and xylem parenchyma, SoPIN1 accumulated in the mature cortex (co) and central pith tissues (p) (Figure 3H, 3K. 15 samples from 4 events). AtPIN1 is not normally observed in the mature cortex or pith tissues (Figure 3G, 3J) (Bennett et al., 2016; Gälweiler et al., 1998). However, we detected abundant AtPIN1 expression in the immature pith closer to the apex (Figure 3D box, Figure 3 – supplement 1 panel D), suggesting that *proAtPIN1* initially drives expression in a broad domain and that AtPIN1 and PIN1b are both cleared from the cortex and pith by maturity, while SoPIN1 is not. In the basal internode all three proteins showed the characteristic rootward polarization pattern regardless of tissue-level abundance (Figure 3 – supplement 1 panels D, E, F arrows).

Taken together, these results show that even under the same transcriptional control AtPIN1, SoPIN1, and PIN1b show distinct tissue-level accumulation patterns in Arabidopsis. While the overall behavior of the two Brachypodium proteins is similar to AtPIN1 in many tissues, there are behaviors unique to each. PIN1b fails to accumulate in epidermal tissues where AtPIN1 and SoPIN1 remain high, whereas SoPIN1 accumulates in the mature cortex and pith tissue where AtPIN1 and PIN1b do not. The

convergent polarization patterns of SoPIN1 and the vascular accumulation of PIN1b in Arabidopsis are remarkably similar to their native behaviors in Brachypodium (O'Connor et al., 2014), suggesting protein-intrinsic features might control tissue level accumulation in the two species.

SoPIN1 but not PIN1b can restore organ initiation and bulk auxin transport in AtPIN1 null mutants

To determine whether the observed differences in SoPIN1 and PIN1b polarization and accumulation have functional consequences in Arabidopsis, we used the *proAtPIN1*-driven SoPIN1 and PIN1b constructs to complement the Arabidopsis *pin1-613* mutant (also known as *pin1-7)*. The *pin1-613* allele is a putative null T-DNA insertion allele with severe organ initiation defects in the inflorescence (Absmanner et al., 2014; Bennett et al., 2006; Smith et al., 2006). Given that epidermal AtPIN1 function is important for organ initiation (Bilsborough et al., 2011; Kierzkowski et al., 2013), as expected only SoPIN1 and not PIN1b was able to complement the *pin1-613* mutation and mediate organ initiation (Figure 4A) (3 out of 6 independent transgenic events showed complementation). However, phenotypic complementation of *pin1-613* by SoPIN1 was incomplete, and mature plants showed a variety of phenotypic defects (Figure 4A, Figure 4 - supplement 1). Most notably, each flower produced more sepals and petals than wild-type but almost no stamens (Figure 4C, Figure 4 - supplement 2). SoPIN1-complemented *pin1-613* plants were thus sterile. We wondered whether these phenotypes could be explained by poor auxin transport function of SoPIN1 in

Arabidopsis. However, SoPIN1 restored wild-type levels of bulk auxin transport to *pin1-613* basal internodes (Figure 4D). Thus, SoPIN1 is capable of supporting organ initiation and mediating rootward auxin transport in the stem, but it is not functionally identical to AtPIN1 expressed under the same promoter.

In SoPIN1-complemented *pin1-613* mutants, SoPIN1 protein accumulation in the meristem epidermis was higher than that observed in a wild-type or heterozygous genetic background, and the pronounced convergent polarization patterns observed in the wild-type background were less defined (Figure 5A, Figure 5 - supplement 1) (16 of 16 meristems). SoPIN1-complemented meristems showed a variety of phyllotactic defects and had highly variable morphologies (Figure 5 – supplement 1 panel B) (16 of 16 meristems). Similar to the pattern observed in the wild-type background, sub-epidermal SoPIN1 in *pin1-613* mutants accumulated in a loosely defined ring within which individual vein traces were difficult to discern (Figure 5I) (13 of 16 meristems). In mature tissues, SoPIN1 accumulated in the epidermis, vasculature, and pith similar to the wild-type background (Figure 5C, 5E, 5G).

In contrast to SoPIN1, PIN1b-expressing *pin1-613* plants had pin-formed inflorescences that were indistinguishable from *pin1-613* alone (Figure 4A) (all 10 expressing events failed to complement). The lack of complementation mediated by PIN1b was not caused by silencing or low expression level because abundant PIN1b signal was observed in *pin1-613* meristems (23 of 26 *pin1-613* meristems from 7 events). In contrast to the wild-type background, most PIN1b expressing *pin1-613* samples had abundant epidermal expression, forming a ring-shaped domain around the meristem apex (Figure 5B, 5D arrow, Figure 5 - supplement 2) (14 of 19 meristems from 6 events). Also unlike

the wild-type background, PIN1b in the epidermis of *pin1-613* meristems was more consistently targeted to the membrane, and was often polar (Figure 5K). However, even with this elevated polar expression in the meristem epidermis, PIN1b was unable to mediate organ initiation in *pin1-613* mutants. Below the apex, PIN1b was polarized rootward in *pin1-613* meristems (Figure 5J), forming defined traces associated with the vasculature (Figure 5F, 5L). In the basal stem of *pin1-613* mutants PIN1b accumulated in a pattern similar to wild-type, although the arrangement of vascular bundles was irregular (Figure 5H). Remarkably, despite clear polar PIN1b expression in *pin1-613* mutant stems (Figure 5M), PIN1b was unable to rescue bulk auxin transport in this tissue (Figure 4D).

Although PIN1b was incapable of supporting organ formation or mediating bulk transport in *pin1-613,* when an auxin maximum was created artificially by addition of lanolin paste infused with IAA, PIN1b epidermal accumulation increased during the initiation of the resultant primordia (Figure 5 – supplement 3) (4 of 6 samples from 2 independent transgenic events). Thus, in the absence of AtPIN1, PIN1b accumulation in the epidermis is still auxin responsive and capable polar localization, but it is not able to mediate organ initiation itself. Consistent with this result, it appears to be unable to transport auxin.

Because PIN1b seemed to form more defined sub-epidermal traces than SoPIN1 (Compare Figure 3 – supplement 1 panels B and C, and Figure 5I and 5L) we thought PIN1b combined with SoPIN1 may improve the partial SoPIN1-mediated complementation of *pin1-613*. We tested two independent PIN1b events for complementation of *pin1-613* when combined with a SoPIN1 event that showed partial

complementation, but all double SoPIN1/PIN1b expressing *pin1-613* plants appeared phenotypically similar to the SoPIN1-only complementation (data not shown). Thus SoPIN1 combined with PIN1b is no better than SoPIN1 alone. In total, these results demonstrate that when expressed in *Arabidopsis,* there is a clear functional separation between SoPIN1 and PIN1b independent of transcriptional control.

SoPIN1 and PIN1b show different behaviors when expressed in the meristem epidermis

Epidermal-specific AtPIN1 expression is sufficient to rescue organ initiation in *atpin1* mutants (Bilsborough et al., 2011), highlighting the importance of AtPIN1 epidermal expression to organ initiation. We wanted to test specifically the ability of SoPIN1 and PIN1b to perform this epidermal function. In order to drive increased PIN1b expression in the epidermis, and to help reduce transgene position-effect variation of expression level, we utilized a two-component expression system in the Landsberg *erecta* (L*er*) background to drive SoPIN1 and PIN1b under the control of the epidermis-enriched Arabidopsis ML1 promoter (Hereafter designated *proAtML1*>>) (Lenhard and Laux, 2003; Sessions et al., 2002). Under the control of *proAtML1* we achieved consistently high epidermal accumulation of both SoPIN1 and PIN1b, but similar to the *proAtPIN1* driven expression described above, only SoPIN1 showed clear convergent polarization patterns around the sites of organ initiation (Figure 6A-6D, Figure 6 supplement 1 and 2) (11 of 11 meristems). Despite consistently high epidermal expression with this system, PIN1b polarity remained difficult to determine, and in many cells the abundance

of protein on the membrane remained low (Figure 6D) (13 of 13 meristems). Instead, PIN1b accumulated in intracellular bodies, especially in the cells of the apical dome and the central domain of initiating organs (Figure 6 – supplement 3 panels A-D). Intracellular PIN1b did not co-localize with early endosomes as assayed by FM4-64 (Figure 6 – supplement 3 panel C arrows), or show the perinuclear localization characteristic of the endoplasmic reticulum, suggesting accumulation in either the golgi apparatus or in vacuoles. PIN1b abundance and polarity was highest at the boundaries of lateral organs (Figure 6 - supplement 2). Thus SoPIN1 and PIN1b show consistent behaviors in the meristem epidermis when expressed under either *proAtPIN1* or *proAtML1.* Despite increased PIN1b expression under *proAtML1,* and a resulting increase in protein accumulation in the apex, PIN1b was still unable to form convergent polarization patterns in wild-type plants.

Both SoPIN1 and PIN1b can rescue the Arabidopsis *pin1-4* mutation when expressed in the meristem epidermis

In order to determine whether the increased PIN1b abundance in the epidermis achieved by the *proAtML1* two-component system had functional consequences, we crossed these transgenes to the *pin1-4* mutant allele. The *pin1-4* allele is in the Landsberg *erecta* (L*er*) background and has a single P579 to L amino acid change in the second-to-last transmembrane domain of AtPIN1 (Bennett et al., 1995), but the phenotype is similarly severe to the null *pin1-613* allele (Figure 7A-C). However, using immuno-localization we detected abundant AtPIN1 protein produced in *pin1-4*

meristems (Figure 7C), while similar to previous authors, we did not detect any protein in pin meristems of the null *pin1-613* allele (Figure 7B) (Absmanner et al., 2014; Bennett et al., 2006) (6 *pin1-613* meristems, 5 *pin1-4* meristems). The AtPIN1 protein detected in *pin1-4* mutants accumulated primarily in the provascular tissues below the pin apex (Figure 7C), and appeared apolar (Figure 7D). Instead, the perinuclear AtPIN1 localization in *pin1-4* suggests accumulation in the endoplasmic reticulum (Figure 7D, arrow). The presence of AtPIN1 protein produced in *pin1-4* mutants indicates that *AtPIN1* in this background may retain partial function despite the severity of the mutant phenotype.

Indeed, both SoPIN1 and PIN1b driven by *proAtML1* were able to rescue the organ formation defects of *pin1-4* (Figure 8A). In contrast to the partial SoPIN1-mediated complementation and failure of PIN1b to complement *pin1-613* described above, both SoPIN1 and PIN1b-complemented *pin1-4* plants made WT flowers that produced seed (Figure 8 – supplement 1). In addition, SoPIN1 and PIN1b were both able to rescue bulk auxin transport in the *pin1-4* basal internode, although PIN1b was less effective than SoPIN1 (Figure 8B). In general SoPIN1 and PIN1b-mediated complementation of *pin1-4* was phenotypically similar, but perhaps as a result of the decreased transport rate in PIN1b-complemented *pin1-4* plants, this genotype showed a significant increase in stem diameter (Figure 8C), providing further evidence that SoPIN1 and PIN1b are not functionally equal.

SoPIN1-complemented *pin1-4* meristems were slightly smaller than wild-type (Figure 6 – supplement 1), but the protein localization was similar to the pattern observed in the WT background, with clear convergent polarization around initiating organs (Figure 6E,

399 6G) (10 of 10 meristems). In contrast, compared to the WT background, PIN1b
400 localization in *pin1-4* was dramatically altered (compare Figure 6B with Figure 6F). Most
401 obvious was an increase in membrane targeted PIN1b and a corresponding reduction in
402 intracellular PIN1b (Figure 6H, Figure 6 supplement 3 panels E-H). PIN1b polarization
403 in the *pin1-4* background was more apparent than in wild-type, and convergent
404 polarization patterns clearly marked incipient organs (Figure 6H) (10 of 10 meristems).
405 PIN1b-complemented meristems accumulated less PIN protein in the apical dome
406 compared to SoPIN1-complemented meristems, and the meristems were larger (Figure
407 6 – supplement 2).

408 In the basal internode, both PINs had similar accumulation patterns in the cortex (co)
409 and epidermis layers (Figure 6I-J arrows), and both showed rootward polarization in the
410 epidermis (Figure 6K-L arrows). Despite this expression domain being drastically
411 different than the wild-type vascular-associated pattern of AtPIN1 (Bennett et al., 2006;
412 Gälweiler et al., 1998), expression in these few cortex layers and epidermis was
413 apparently sufficient to drive near wild-type levels of rootward bulk auxin transport in
414 *pin1-4* (Figure 8B). Thus, while both proteins can complement the *pin1-4* organ initiation
415 phenotype, the SoPIN1 and PIN1b complemented lines have differing localization
416 patterns, slightly different auxin transport properties, and minor differences in meristem
417 and mature plant morphologies, suggesting once again that SoPIN1 and PIN1b are not
418 functionally identical.

419

420

Discussion

The SoPIN1 and PIN1 clades have different functions in Brachypodium

During spikelet development in Brachypodium, SoPIN1 forms convergent polarization patterns surrounding the sites of organ initiation and strong expression of the auxin response reporter DR5 (O'Connor et al., 2014). We provide additional evidence here that SoPIN1 polarizes towards sites of high auxin concentration by showing that a DII minimum occurs at SoPIN1 convergence points. In *sopin1* mutants the reduction of DII does not occur, suggesting that SoPIN1 functions to concentrate auxin at epidermal maxima, and similar to Arabidopsis, this is required for organ initiation in the inflorescence. The barren inflorescence phenotype of *sopin1-1* mutants, and the specificity of SoPIN1 for the outer tissues and for convergent polarization patterns in Brachypodium provides further support for the idea that auxin maximum formation is necessary for organ initiation, and that this is primarily mediated by convergent PIN in the meristem epidermis (Bhatia et al., 2016; Jönsson et al., 2006; Kierzkowski et al., 2013; Smith et al., 2006).

SoPIN1 clade mutants have been reported in the legume *Medicago truncatula* and in tomato (*Solanum lycopersicum*), and these mutants show pleiotropic phenotypes involving phyllotaxy, organ initiation, inflorescence branching, leaf serrations, and leaf compounding, but they do not form barren pin meristems (Martinez et al., 2016; Zhou et al., 2011). These wider morphogenetic events also involve epidermal PIN convergence points and associated auxin maxima (Barkoulas et al., 2008; Bilsborough et al., 2011),

443 suggesting a general role for SoPIN1 clade members in generating such maxima. The
444 lack of barren pin-formed meristems in these mutants suggests that different species
445 are variably dependent on SoPIN1-generated auxin maxima for organ initiation. Even in
446 Brachypodium and Arabidopsis, barren meristems in *sopin1* and at*pin1* respectively are
447 restricted to later stages of development, so organs are able to form in the absence of
448 SoPIN1 or AtPIN1 function.

449 In contrast to *sopin1* mutants, loss of *pin1* clade function in Brachypodium has very little
450 effect on organ initiation, despite both PIN1a and PIN1b being expressed and polarized
451 away from auxin maxima in developing organs (O'Connor et al., 2014). Auxin drainage
452 is thought necessary for proper organ size and placement (Bhatia et al., 2016; Deb et
453 al., 2015), but the most evident phenotype in *pin1a/pin1b* mutants is the alteration of
454 internode length. The increased internode length in *pin1b,* and severely reduced
455 internode length in *pin1a/pin1b* double mutants, provides new genetic tractability to
456 address how PINs regulate tissue growth in the shoot independent of organ initiation, a
457 PIN function that is experimentally inaccessible in Arabidopsis because of the initiation
458 defects of *atpin1* mutants.

459 Grasses contain intercalary meristems, bands of indeterminate tissue separated from
460 the apical meristem that are responsible for internode growth after organ initiation.
461 Auxin dynamics in this more basal meristematic tissue may be important for controlling
462 stem growth. Indeed**,** loss of the ABCB1 auxin exporter in maize and Sorghum results in
463 dwarfism associated with reduced activity of intercalary meristems (Knöller et al., 2010;
464 Multani et al., 2003). The role of PIN1a and PIN1b in regulating intercalary meristem

growth will be an important avenue for future work, especially since plant stature has played such an important role in grass domestication.

The properties that define PIN behavior and function

Membrane accumulation. We used heterologous expression of SoPIN1 and PIN1b in Arabidopsis to explore the ways in which different PIN family members may have different properties post-transcription (Summarized in Figure 9). When expressed in the meristem epidermis in wild-type Arabidopsis, SoPIN1 is localized to the membrane in most cells while PIN1b often accumulates internally (Figure 6 - supplement 3). Thus, with the same transcriptional control, different PINs can vary in the degree to which, after protein production, they accumulate at the plasma membrane. The differential membrane targeting of PIN1b and SoPIN1 is a tissue-specific phenomenon however, because unlike in the epidermis, in the basal internode both PINs accumulate at the rootward plasma membrane (Figure 3 - supplement 1 panels E and F). The regulation of PIN plasma membrane polar targeting and endocytic recycling has been an important avenue for understanding PIN function and general membrane protein biology (Luschnig and Vert, 2014). Our results provide further evidence that at least some of the signals governing membrane accumulation are inherent in, and vary between, different PIN family members (Wisniewska et al., 2006).

Tissue accumulation. Under the same transcriptional control AtPIN1, SoPIN1, and PIN1b show different tissue-level accumulation patterns in Arabidopsis. In wild-type plants, *proAtPIN1*-expressed PIN1b shows reduced overall accumulation in the

epidermis compared to AtPIN1 or SoPIN1 (Compare Figure 3D-3F). Even with greater expression under *proAtML1,* the intracellular PIN1b signal observed in the meristem epidermis (Figure 6 - supplement 3) suggests that PIN1b protein could be actively targeted to the vacuole for degradation as has been shown for PIN2 in the root (Abas et al., 2006; Kleine-Vehn et al., 2008b). In contrast, SoPIN1 is abundant in the meristem epidermis and accumulates in the mature cortex and pith tissues where AtPIN1 and PIN1b do not (Figure 3H arrows). Because we observed clear AtPIN1 accumulation in the immature pith (Figure 3 - supplement 1 panel D), this suggests that *proAtPIN1* is at least initially active in pith tissue and that the PIN1 clade members, AtPIN1 and PIN1b, are removed later in development, while SoPIN1 is not. Laser capture micro-dissection and RNAseq of mature stem tissue has detected abundant *AtPIN1* transcription in the mature pith (T. Greb, personal communication, February 2017), suggesting that even at maturity AtPIN1, and probably PIN1b are actively cleared post-transcriptionally from this tissue. Our results suggest that the AtPIN1 expression domain is far broader than is indicated by the protein accumulation pattern, and further highlight the importance of PIN post-transcriptional regulation for controlling PIN tissue-level abundance.

In Arabidopsis, endogenous PIN family members show a degree of cross-regulation where loss-of-function mutations in one PIN family member result in tissue-level accumulation of a different PIN in a compensatory pattern (Blilou et al., 2005; Paponov et al., 2005; Vieten et al., 2005). We observed similar behavior in the *pin1-613* null background, where SoPIN1 and PIN1b accumulation in the meristem epidermis was increased in the absence of AtPIN1 (Figure 5 supplements 1 and 2). This sensitivity of SoPIN1 and PIN1b to the presence of AtPIN1, even while under the *AtPIN1* promoter,

suggests that wild-type AtPIN1 is able to compete with SoPIN1 and PIN1b post-transcriptionally for residency at the membrane. However, we did not observe the same competitive effect with *proAtML1* where SoPIN1 and PIN1b tissue-level accumulation, though not membrane residence, seemed similar between *pin1-4* mutant and wild-type meristems (Figure 6 - supplements 1 and 2). This difference between *proAtPIN1* and *proAtML1* may be because PIN transcription under *proAtPIN1* is sensitive to the dosage of other PINs as has been suggested (Vieten et al., 2005). Alternatively, the lack of increased SoPIN1 and PIN1b accumulation in the *pin1-4* mutant background may be because the AtPIN1 protein produced in *pin1-4* is still able to compete with the other expressed PINs. Regardless, these results highlight the sensitivity of PIN tissue-level abundance to both transcriptional and post-transcriptional control, and the variability between PIN family members independent of transcription.

Transport activity. In Arabidopsis, phosphorylation of PINs by several different families of protein kinases is thought necessary for efficient auxin transport (Absmanner et al., 2014; Barbosa et al., 2014; Jia et al., 2016; Willige et al., 2013). PIN activation by phosphorylation may explain the inability of PIN1b to mediate bulk auxin transport in the basal internode of *pin1-613* plants despite being expressed, accumulating at the membrane, and being polarized rootward in this tissue (Figure 4D, Figure 5M). It is possible that in the *proAtPIN1* domain PIN1b does not interact with the appropriate activating kinase, and it is thus unphosphorylated and inactive. Indeed, a partially unphosphorylatable form of AtPIN1 fails to complement fully the bulk auxin transport defect of *pin1-613* mutants in the basal internode (Absmanner et al., 2014), and AtPIN1

polarity can be uncoupled from phosphorylation status, and thus presumably transport activity can be independent of polarization (Weller et al., 2017).

However, when expressed using *proAtML1,* PIN1b expression in the outer tissue layers of the basal internode appears sufficient to mediate bulk auxin transport in *pin1-4* (Figure 8B). One explanation for this is that PIN1b activity may be tissue dependent, perhaps because of the differing expression domains of activating kinases (Absmanner et al., 2014). Arabidopsis PIN4 and PIN7 are present in the *proAtML1* domain (Bennett et al., 2016), making it conceivable that these PINs are the normal targets of activating kinases in this tissue. Alternatively, kinases in the L*er* genetic background may be more effective at activating PIN1b than those in Col, but the dramatic effect of the *pin1-4* allele vs wild-type *AtPIN1* on PIN1b polarization behavior within the L*er* background makes this explanation unlikely (see below). In either case, the behavior of PIN1b in *pin1-613* provides a clear indication that even once a PIN has accumulated at the cell membrane in a tissue it may not be active.

Interaction. A particularly striking result is the ability of PIN1b to form convergent polarization patterns and mediate organ initiation in the *pin1-4* missense mutant background when it is unable to do so in the null *pin1-613* background. It is unlikely that differences between *proAtPIN1* and *proAtML1*-mediated expression can explain this differential complementation because both promoters drive expression in the epidermis, and both promoters are sufficient to complement *atpin1* mutants using wild-type AtPIN1 as well as SoPIN1. As described above, it is possible that differences in activating enzymes or similar interactors between the L*er* and Col backgrounds could contribute to the strikingly different behavior of PIN1b in *pin1-4* vs *pin1-613*. Indeed, mutation of the

leucine-rich repeat receptor-like kinase *ERECTA,* which is mutated in the L*er* background, has known effects on PIN1 localization when combined with other mutations in the *ERECTA* family (Chen et al., 2013; Torii et al., 1996). However, the dramatic effect of wild-type AtPIN1 vs *pin1-4* on PIN1b membrane targeting (compare Figure 6 - supplement 3 panels A-D to E-H) within the L*er* background suggests the differing genetic backgrounds of each complementation (L*er* vs Col-0) is not sufficient to explain the differential complementation.

Instead, the strong influence of *pin1-4* on PIN1b membrane targeting and polarity in the meristem epidermis suggests that PIN1b may be cooperating with a partially functional *pin1-4* protein and together they recapitulate the organ initiation functions of wild-type AtPIN1. PIN1b interaction with *pin1-4* in the outer cortex of the stem may also explain the ability of PIN1b to rescue bulk transport in the basal internodes of *pin1-4* mutants while it cannot in the null *pin1-613* allele. Partial *pin1-4* function is further supported by the result that SoPIN1 complementation of the null *pin1-613* allele is incomplete, and because of flower defects the plants are sterile (Figure 4C), while SoPIN1-mediated complementation of *pin1-4* is complete, and flowers are phenotypically normal and set seed (Figure 8 - supplement 1). Accordingly, SoPIN1 convergent polarization patterns are more evident in the presence of *pin1-4* than they are during complementation of the null *pin1-613* allele (Compare 5A and 6E), further evidence that residual *pin1-4* function augments SoPIN1 during *pin1-4* complementation. Combined, these data suggest that the *pin1-4* allele is hypomorphic, and that it provides some necessary function to PIN1b.

If PIN1b is indeed inactive in null *pin1-613* mutants as we hypothesized above, then it is possible *pin1-4* facilitates the interaction of PIN1b with the appropriate activating kinase,

578 and this allows PIN1b to perform organ initiation and bulk transport. Alternatively,
579 interaction between PIN1b and *pin1-4* may facilitate proper membrane targeting or
580 polarization of either protein, resulting in functional transport. The increased level of
581 polar, plasma-membrane localized PIN1b in *pin1-4* meristems supports the idea that
582 *pin1-4* controls PIN1b membrane residency, but it cannot explain why PIN1b appears
583 unable to mediate bulk transport in *pin1-613* despite being membrane-localized and
584 polar in the basal internode.

585 Direct PIN-PIN interactions have so far not been shown, but if one PIN type can convey
586 targeting, polarity, or activity information to another through direct or indirect interaction,
587 this may be relevant to auxin transport in tissues where multiple PINs are coexpressed,
588 such as in the Arabidopsis root meristem (Blilou et al., 2005), or in the shoot apical
589 meristems of most angiosperms where the SoPIN1 and PIN1 clade proteins likely
590 overlap, as they do during spikelet development in Brachypodium (O'Connor et al.,
591 2014).

592 **Polarity.** We previously showed that the polarization dynamics of SoPIN1, PIN1a, and
593 PIN1b in *Brachypodium* could be modeled by assigning two different polarization modes
594 to the SoPIN1 and PIN1 clades (O'Connor et al., 2014). In the model, SoPIN1 orients
595 toward the adjacent cell with the highest auxin concentration, thus transporting auxin up
596 the concentration gradient and providing a positive feedback to concentrate auxin into
597 local maxima. In contrast, in the model, PIN1a and PIN1b proteins are allocated in
598 proportion to net auxin flux, thus providing a positive feedback in which flux through the
599 tissue is amplified by the allocation of PIN1a/b in the direction of that flux. The
600 assignment of two different polarization modes was previously used to describe the

601 behavior of AtPIN1 during organ placement and vein patterning using an auxin-
602 concentration based switching mechanism between the up-the-gradient (UTG) and with-
603 the-flux (WTF) polarization modes (Bayer et al., 2009). However, it has also been
604 suggested that a flux-based mechanism alone can account for both convergence points
605 and vein patterning (Abley et al., 2016; Stoma et al., 2008).

606 Despite evidence that convergent PIN polarization is dependent on localized auxin
607 signaling in adjacent cells (Bhatia et al., 2016), there are still no proven mechanisms for
608 direct sensing of intercellular auxin gradients or auxin fluxes across membranes. The
609 *sopin1, pin1a,* and *pin1b* phenotypes in Brachypodium are consistent with different
610 polarization modes. SoPIN1 is required for organ initiation and the formation of auxin
611 maxima in Brachypodium, which is primarily modeled using UTG polarization (Bayer et
612 al., 2009; Jönsson et al., 2006; Smith et al., 2006). On the other hand, *pin1a* and *pin1b*
613 mutant plants do not show organ initiation defects, but rather only have internode
614 elongation defects, a tissue where WTF models have been used to explain PIN
615 dynamics and measured auxin transport kinetics during vein patterning and the
616 regulation of branch outgrowth (Bayer et al., 2009; Bennett et al., 2016; Mitchison,
617 1980; Mitchison et al., 1981; Prusinkiewicz et al., 2009).

618 In wild-type Brachypodium, the SoPIN1 and PIN1a/b expression domains are almost
619 entirely mutually exclusive (O'Connor et al., 2014), making it possible that the observed
620 polarization differences between the two clades are due to expression context or tissue-
621 level stability, and not to functional differences between the proteins themselves. More
622 specifically, perhaps an UTG mechanism dominates the epidermis while a WTF
623 mechanism is utilized in the internal tissues, and different PINs interact equally with

624 these context-dependent mechanisms. Our heterologous expression studies do not
625 exclusively support context-dependent or protein-dependent mechanisms for SoPIN1
626 and PIN1 polarization. It is clear that alone only SoPIN1 and AtPIN1 show the
627 convergent polarization patterns associated with UTG polarization, and alone only
628 SoPIN1 and AtPIN1 are thus able to mediate organ initiation, while PIN1b cannot. On
629 the other hand, all three PINs are capable of rootward polarization in the basal
630 internode tissue, and PIN1b can be co-opted to convergent polarization at the meristem
631 epidermis in the presence of *pin1-4*. The results presented here do not demonstrate
632 whether within a single cell SoPIN1 and PIN1b would orient differently with respect to
633 auxin as might be expected for the dual polarization model (O'Connor et al., 2014).
634 However, such context-independent polarization behavior was previously observed for
635 PIN1 and PIN2 in the root where both PINs can polarize in opposing directions within a
636 single cell type when expressed in the PIN2 domain (Kleine-Vehn et al., 2008a;
637 Wisniewska et al., 2006).

638 ## Outlook

639 In total, our Brachypodium mutant phenotypes and heterologous expression results
640 point to multiple levels at which PIN family members can be functionally distinct.
641 Differential membrane targeting, tissue level accumulation, transport activity, indirect or
642 direct interaction, and the resultant polarity may all contribute to the dynamics of PIN
643 action during plant development. In most flowering plants two PIN clades, SoPIN1 and
644 PIN1, with differing functions and differing transcriptional and post-transcriptional
645 properties mediate auxin transport in the shoot, but these properties are seemingly
646 combined into AtPIN1 in Arabidopsis and other Brassicaceae species. Because PIN1b

alone is unable to mediate organ initiation while AtPIN1 can, and these two PINs are both members of the same clade, AtPIN1 may have gained the ability to form convergent polarization patterns and mediate organ initiation after, or coincident with, the loss of the SoPIN1 clade. Indeed, when comparing Brassicaceae PIN1 proteins against a broad sampling of other angiosperm PIN1 proteins, the Brassicaceae PIN1 proteins have several divergent protein domains (Figure 9 - supplement 1), suggesting possible neofunctionalization within the Brassicacea family. Alternatively, an expansion of the PIN3,4,7 clade is also characteristic of Brassicacea species (Bennett et al., 2014; O'Connor et al., 2014), making it possible duplicated members of this clade buffered the loss of SoPIN1. However, there is no indication that PIN3,4,7 have a role in organ initiation in the inflorescence (Guenot et al., 2012). Regardless, we believe the combination of SoPIN1 and PIN1 characteristics into AtPIN1 coincident with the loss of the SoPIN1 clade represents a form of reverse-subfunctionalization, the combination of functions originally split between homologs into a single protein after gene loss. It is not surprising that PINs may be particularly amenable to this kind of functional evolution because, as described above, there are several post-transcriptional regulatory steps that ultimately combine to control PIN function in plants. The output of auxin transport is the sum of an extensive network of post-transcriptional interactions that all act to regulate auxin transport itself, and this gives the system plasticity during development, and perhaps also over evolutionary time.

Materials and Methods

sopin1-1, *pin1a-1,* and *pin1b-1* creation with CRISPR

SoPIN1 (Bradi4g26300), PIN1a (Bradi1g45020), and PIN1b (Bradi3g59520) were targeted with CRISPR using vectors developed for rice (Miao et al., 2013). CRISPR constructs were transformed into Brachypodium inbred line Bd21-3 using previously published methods (Bragg et al., 2015).

sopin1-1 CRISPR

The SoPIN1 guide was AGGCTGTCGTACGAGGAGT. This guide was shorter than the typical 20bp in an effort to provide greater target specificity for SoPIN1 (Fu et al., 2014). In the T0 regenerated plants, 5 out of 9 independent transgenic events showed severe organ initiation defects, and all 5 contained lesions in the SoPIN1 CRIPSR target site. Unfortunately, only one of the events with a T0 phenotype set seed. In the T1 progeny of this event only those individuals that contained the CRISPR transgene showed lesions in the SoPIN1 CRISPR target site, and these plants showed the *sopin1* phenotype and thus failed to set seed, suggesting active editing by the SoPIN1 CRISPR transgene in this event.

Not all events showed such efficient editing however, and we identified an independent T1 family where a C insertion in the SoPIN1 CRISPR target site co-segregated with the barren inflorescence phenotype. We designated this allele, which causes a premature stop codon before the end of the third exon codon 739 base pairs downstream from the target site, *sopin1-1*. (Primer IDs 1-2 Table 1) We backcrossed a heterozygous *sopin1-1*

plant to the Bd21-3 parental line and all F1 progeny (N=4) were wild-type. In the F2 generation, plants homozygous for the *sopin1-1* lesion co-segregated with the barren inflorescence phenotype (N=60: 32 het, 18 homo,10 wt). Amongst these plants, 16 did not have the Cas9 transgene (Primer IDs 3-4 Table 1), and the barren inflorescence phenotype still co-segregated with the *sopin1-1* lesion (N=16: 8 het, 3 homo, 5 wt). We crossed the T1 *sopin1-1* heterozygous plant with a line homozygous for the previously published SoPIN1-CITRINE genomic reporter line (O'Connor et al., 2014). In the F2 we identified families homozygous for *sopin1-1* but segregating for the SoPIN1-CITRINE transgene. Only individuals that lacked the SoPIN1-CITRINE transgene showed a *sopin1-1* phenotype, while those that contained the SoPIN1-CITRINE transgene made spikelets and set seed (Figure 1 - supplement 1). This complementation was independent of the presence of Cas9.

pin1a-1 CRISPR

The PIN1a guide was ATCTACTCCCGGCGGTCCAT. We identified edited plants in the T1 generation (Primer IDs 5-6 Table 1), then found a homozygous T insertion in the T2 generation which was independent of Cas9, resulting in a premature stop codon 939 base pairs downstream, here designated *pin1a-1*. No single-mutant *pin1a-1* phenotypes were observed.

pin1b-1 CRISPR

The PIN1b guide was AGGGCAAGTACCAGATCC. We identified a single plant from the regenerating T0 PIN1b CRISPR population that had longer basal internodes and twisted leaves. This plant was homozygous for an A deletion in the PIN1b CRISPR

target site causing a premature stop in the second exon 502 base pairs downstream, here designated *pin1b-1* (Primer IDs 7-8 Table 1). All T1 progeny showed the *pin1b* phenotype and were homozygous for the *pin1b-1* lesion. We backcrossed these T1 plants to Bd21-3 and all F1 progeny had a wild-type phenotype (N=11). In the F2, the *pin1b* phenotype co-segregated with the *pin1b-1* lesion (N= 215, 91 het, 39 homo, 26 wt). Amongst these plants, 24 did not have the Cas9 transgene, and the *pin1b* phenotype still co-segregated perfectly with the *pin1b-1* lesion (N=24: 10 het, 6 homo, 8 wt). We crossed *pin1b-1* without Cas9 to a line homozygous for the previously published PIN1b-CITRINE transgene (O'Connor et al., 2014). In the F3 we identified lines homozygous for both the transgene and *pin1b-1* and used these to quantify internode lengths compared to *pin1b-1* (Figure 2 - supplement 1).

pin1a-1 / pin1b-1 double mutant.

Homozygous *pin1b-1* lacking Cas9 was crossed to homozygous *pin1a-1* lacking Cas9. In the F2 phenotypically *pin1b-1* plants that were also genotyped heterozygous for *pin1a-1* were identified. In the homozygous *pin1b-1* F3 generation the double *pin1a-1 / pin1b-1* mutant phenotype segregated perfectly with the *pin1a-1* lesion (N=2: 10 het, 5 homo, 8 wt). Double *pin1a-1 / pin1b-1* mutants were easily identified by phenotype and produce seed.

Brachypodium Reporter Constructs

All constructs were cloned using Multi-site Gateway (Invitrogen) and were transformed into Brachypodium Bd21-3 using previously published methods (Bragg et al., 2015). For pZmUbi::DII-Venus, we first cloned the maize ubiquitin promoter into pDONR P4-P1R

(Primer IDs 9-10 Table 1) and this was subsequently recombined with pDONR 221 containing Arabidopsis DII and pDONR P2R-P3 containing VENUS-N7 (Brunoud et al., 2012) into the Multi-site Gateway binary vector pH7m34GW (http://gateway.psb.ugent.be/). In the T3 generation, degradation of DII-Venus in the presence of auxin was validated by treating excised Brachypodium spikelet meristems with 1 µM 1-naphthaleneacetic acid (NAA) or mock treatment in 70% ethanol, and imaging every 30 min (Figure 1 –supplement 2).

For SoPIN1-Cerulean, the promoter plus 5' coding pDONR-P4-P1R and 3' coding plus downstream pDONR-P2R-P3 fragments from (O'Connor et al., 2014) were used. Maize codon-optimized Cerulean florescent protein, courtesy of David Jackson, was amplified with 5x Ala linkers and cloned into pENTR/D-TOPO. These three fragments were then recombined into pH7m34GW.

Arabidopsis Reporter Constructs

All constructs were cloned using Multi-site Gateway (Invitrogen) and transformed using standard floral dip. For *proAtPIN1* complementation, a 3.5kb Arabidopsis PIN1 promoter region was amplified from a genomic clone previously reported to complement the *pin1* (Heisler et al., 2005) and cloned into Gateway vector pDONR P4-P1R (Primer IDs 11-12 Table 1). For each Brachypodium PIN-CITRINE fusion construct, the entire PIN coding region, including the CITRINE insertion, was amplified from the previously published reporter constructs (O'Connor et al., 2014) and cloned into pENTR /D-TOPO (Primer IDs 13-16 Table 1). The CITRINE fusion in each is located in a position known to complement *pin1* mutations (Heisler et al., 2010; Wisniewska et al., 2006; Xu et al.,

2006). The *proAtPIN1* pDONR P4-P1R and PIN coding region pENTR/D-TOPO vectors were then recombined into Gateway binary vector pH7m24GW (http://gateway.psb.ugent.be/) and transformed by floral dip into both Col-0 and plants heterozygous for *pin1-613* (also known as *pin1-7,* SALK_047613) (Bennett et al., 2006; Smith et al., 2006). Complementation was assessed in the T3 generation, and all plants were genotyped for both the *pin1-613* mutation (Primer IDs 17-19 Table 1) and for presence of the PIN transgene (Primer IDs 20-22 Table 1).

For the *proAtML1* lines the PIN coding regions with CITRINE insertion pENTR /D-TOPO Gateway vectors were recombined downstream of the two-component OP promoter in vector pMoA34-OP (Moore et al., 1998) and then transformed into the *proAtML1* driver line in the Landsberg *erecta* background (Lenhard and Laux, 2003). Lines homozygous for both the *proAtML1* driver and OP::PIN were crossed to het *pin1-4* and complementation was assessed in the F2 and F3 generations. All complemented plants were genotyped for *pin1-4* (Primer IDs 23-24 Table 1), the Brachypodium PINs (Primer IDs 20-22 Table 1), and the presence of the ML1 driver transgene (Primer IDs 25-26 Table 1).

Confocal and Scanning Electron Microscopy

All confocal images were captured on a Zeiss 780 laser scanning confocal using a W Plan-Apochromat 20x or 63x magnification 1.0 numerical aperture objectives. Detection wavelengths: 517-570nm for CITRINE-tagged PINs, 535-552 for DII-Vinus, 463-509 for SoPIN1-CERULEAN, 490-543 for AtPIN1-GFP, 691-753nm for FM4-64, 561-606nm for Dylight 549, 631-717nm for Propidium Iodide, and 646-726 for chlorophyll A auto-

778 fluorescence. The pinhole was set to 1 airy unit for all meristem stacks and details of
779 sub-epidermal polarization, but was open to the maximum setting for tiled longitudinal
780 and cross sections of the basal internode (Figures 3D-L, 5C-H and 6I-J). Detection gain
781 and laser power were varied according to signal strength unless direct comparisons
782 between genotypes were made as indicated in figure legends.

783 Cryo scanning electron microscopy was performed on a Zeiss EVO HD15 SEM fitted
784 with a LaB6 filament and a Quorum PP3010T (Quorum Technololgies, Lewes, Sussex.
785 UK) cryo preparation unit using the BSD (Backscattered electron) detector with probe
786 current as set to 10 nA, and 15.00 kV gun voltage. Frozen samples were coated in
787 <1.5nm Pt.

788 Auxin Transport Assays

789 Auxin transport assays were carried out as described in (Crawford et al., 2010). Briefly,
790 17 mm long basal internodes were excised and the apical end submerged in 30 µl
791 Arabidopsis salts (ATS) without sucrose (pH = 5.6) containing 1 µM ^{14}C-IAA (American
792 Radiolabeled Chemicals). After 6 hours incubation, the basal 5 mm segment was
793 excised, cut in half, and shaken overnight at 400 RPM in 200 µl scintillation liquid prior
794 to scintillation counting. 10µM N-1-Naphthylphthalamic Acid (NPA), an auxin transport
795 inhibitor, was added prior to incubation for negative controls.

796 AtPIN1 Immuno-Localization

797 Detection of AtPIN1 in sectioned apexes was performed as previously described
798 (O'Connor et al., 2014). Commercial polyclonal goat anti-AtPIN1 (AP-20) was used at a

concentration of 1:150 (Santa Cruz Biotechnology). Affinity-purified Donkey Anti-Goat Dylight 549 secondary was used at a concentration of 1:200 (Jackson Immuno Research). Control samples where the primary antibody was omitted showed a similar level of background signal as *pin1-613* null mutant samples.

Acknowledgments

Thanks to Raymond Wightman for SEM assistance, Martin van Rongen for assistance with transport assays and *pin1-613* oligos, Tom Bennett for *proAtPIN1* oligos, Marcus Heisler for AtPIN1-GFP construct and *pin1-4* genotyping assistance, Teva Vernoux for DII plasmids, David Jackson for maize codon-optimized Cerulean, and to all the members of the Leyser lab. Thanks also to Graeme Mitchison, Katie Abley, Michael Raissig, and Pau Formosa-Jordan for helpful comments on the manuscript.

Competing interests

The authors have no competing interests.

References

Abas, L., Benjamins, R., Malenica, N., Paciorek, T., Wisniewska, J., Wirniewska, J., Moulinier-Anzola, J. C., Sieberer, T., Friml, J. and Luschnig, C. (2006). Intracellular trafficking and proteolysis of the Arabidopsis auxin-efflux facilitator PIN2 are involved in root gravitropism. *Nat*

820 *Cell Biol* **8**, 249–256.

821 **Abley, K., Marée, A. F. and Coen, E.** (2016). Formation of polarity
822 convergences underlying shoot outgrowths. *eLife* **5**, 2061.

823 **Absmanner, B., Barbosa, I. C. R., Willige, B. C., Fastner, A., Streit, V., Port,**
824 **S. A. and la Fuente van Bentem, de, S.** (2014). Auxin efflux by PIN-
825 FORMED proteins is activated by two different protein kinases, D6 PROTEIN
826 KINASE and PINOID. *eLife* **3**.

827 **Adamowski, M. and Friml, J.** (2015). PIN-Dependent Auxin Transport: Action,
828 Regulation, and Evolution. *The Plant Cell* **27**, 20–32.

829 **Barbosa, I. C. R., Zourelidou, M., Willige, B. C., Weller, B. and**
830 **Schwechheimer, C.** (2014). D6 PROTEIN KINASE activates auxin transport-
831 dependent growth and PIN-FORMED phosphorylation at the plasma
832 membrane. *Dev Cell* **29**, 674–685.

833 **Barkoulas, M., Hay, A., Kougioumoutzi, E. and Tsiantis, M.** (2008). A
834 developmental framework for dissected leaf formation in the Arabidopsis
835 relative Cardamine hirsuta. *Nat Genet* **40**, 1136–1141.

836 **Bayer, E. M., Bayer, E. M., Smith, R. S., Mandel, T., Nakayama, N., Sauer, M.,**
837 **Prusinkiewicz, P. and Kuhlemeier, C.** (2009). Integration of transport-based
838 models for phyllotaxis and midvein formation. *Genes Dev* **23**, 373–384.

839 **Benková, E., Michniewicz, M., Sauer, M., Teichmann, T., Seifertová, D.,**
840 **Jürgens, G. and Friml, J.** (2003). Local, Efflux-Dependent Auxin Gradients
841 as a Common Module for Plant Organ Formation. *Cell* **115**, 591–602.

842 **Bennett, S. R. M., Alvarez, J., Bossinger, G. and Smyth, D. R.** (1995).
843 Morphogenesis in pinoid mutants of Arabidopsis thaliana. *Plant J* **8**, 505–520.

844 **Bennett, T. A., Brockington, S. F., Rothfels, C., Graham, S. W., Stevenson,**
845 **D., Kutchan, T., Rolf, M., Thomas, P., Wong, G. K.-S., Leyser, H. M. O., et**
846 **al.** (2014). Paralogous radiations of PIN proteins with multiple origins of
847 noncanonical PIN structure. *Molecular Biology and Evolution* **31**, 2042–2060.

848 **Bennett, T. A., Hines, G., van Rongen, M., Waldie, T., Sawchuk, M. G.,**
849 **Scarpella, E., Ljung, K. and Leyser, H. M. O.** (2016). Connective Auxin
850 Transport in the Shoot Facilitates Communication between Shoot Apices.
851 *PLoS Biol* **14**, e1002446.

852 **Bennett, T. A., Sieberer, T., Willett, B., Booker, J., Luschnig, C. and Leyser,**
853 **H. M. O.** (2006). The Arabidopsis MAX Pathway Controls Shoot Branching by

Regulating Auxin Transport. *Current Biology* **16**, 553–563.

Bhatia, N., Bozorg, B., Larsson, A., Ohno, C., Jönsson, H. and Heisler, M. G. (2016). Auxin Acts through MONOPTEROS to Regulate Plant Cell Polarity and Pattern Phyllotaxis. *Curr Biol* **26**, 3202–3208.

Bilsborough, G. D., Runions, A., Barkoulas, M., Jenkins, H. W., Hasson, A., Galinha, C., Laufs, P., Hay, A., Prusinkiewicz, P. and Tsiantis, M. (2011). Model for the regulation of Arabidopsis thaliana leaf margin development. *Proc Natl Acad Sci USA* **108**, 3424–3429.

Blilou, I., Xu, J., Wildwater, M., Willemsen, V., Paponov, I., Friml, J., Heidstra, R., Aida, M., Palme, K. and Scheres, B. (2005). The PIN auxin efflux facilitator network controls growth and patterning in Arabidopsis roots. *Nature* **433**, 39–44.

Bragg, J. N., Anderton, A., Nieu, R. and Vogel, J. P. (2015). Brachypodium distachyon. *Methods Mol Biol* **1223**, 17–33.

Brunoud, G., Wells, D. M., Oliva, M., Larrieu, A., Mirabet, V., Burrow, A. H., Beeckman, T., Kepinski, S., Traas, J., Bennett, M. J., et al. (2012). A novel sensor to map auxin response and distribution at high spatio-temporal resolution. *Nature* **482**, 103–106.

Chen, M.-K., Wilson, R. L., Palme, K., Ditengou, F. A. and Shpak, E. D. (2013). ERECTA family genes regulate auxin transport in the shoot apical meristem and forming leaf primordia. *Plant Physiol* **162**, 1978–1991.

Crawford, S., Shinohara, N., Sieberer, T., Williamson, L., George, G., Hepworth, J., Muller, D., Domagalska, M. A. and Leyser, H. M. O. (2010). Strigolactones enhance competition between shoot branches by dampening auxin transport. *Development* **137**, 2905–2913.

Deb, Y., Marti, D., Frenz, M., Kuhlemeier, C. and Reinhardt, D. (2015). Phyllotaxis involves auxin drainage through leaf primordia. *Development* **142**, dev.121244–2001.

Derbyshire, P. and Byrne, M. E. (2013). MORE SPIKELETS1 is required for spikelet fate in the inflorescence of Brachypodium. *Plant Physiol* **161**, 1291–1302.

Fu, Y., Sander, J. D., Reyon, D., Cascio, V. M. and Joung, J. K. (2014). Improving CRISPR-Cas nuclease specificity using truncated guide RNAs. *Nat Biotechnol* **32**, 279–284.

888 **Gälweiler, L., Guan, C., Müller, A., Wisman, E., Mendgen, K., Yephremov, A. and Palme, K.** (1998). Regulation of Polar Auxin Transport by AtPIN1 in
890 Arabidopsis Vascular Tissue. *Science* **282**, 2226–2230.

891 **Gordon, S. P., Heisler, M. G., Reddy, G. V., Ohno, C., Das, P. and Meyerowitz, E. M.** (2007). Pattern formation during de novo assembly of the
893 Arabidopsis shoot meristem. *Development* **134**, 3539–3548.

894 **Guenot, B., Bayer, E. M., Bayer, E., Kierzkowski, D., Smith, R. S., Mandel, T., Zádníková, P., Benková, E. and Kuhlemeier, C.** (2012). Pin1-independent
896 leaf initiation in Arabidopsis. *Plant Physiol* **159**, 1501–1510.

897 **Habets, M. E. J. and Offringa, R.** (2014). PIN-driven polar auxin transport in
899 plant developmental plasticity: a key target for environmental and endogenous signals. *New Phytologist* **203**, 362–377.

900 **Heisler, M. G., Hamant, O., Krupinski, P., Uyttewaal, M., Ohno, C., Jönsson, H., Traas, J. and Meyerowitz, E. M.** (2010). Alignment between PIN1 polarity
902 and microtubule orientation in the shoot apical meristem reveals a tight
903 coupling between morphogenesis and auxin transport. *PLoS Biol* **8**,
904 e1000516.

905 **Heisler, M. G., Ohno, C., Das, P., Sieber, P., Reddy, G. V., Long, J. A. and Meyerowitz, E. M.** (2005). Patterns of auxin transport and gene expression
907 during primordium development revealed by live imaging of the Arabidopsis
908 inflorescence meristem. *Curr Biol* **15**, 1899–1911.

909 **Jia, W., Li, B., Li, S., Liang, Y., Wu, X., Ma, M., Wang, J., Gao, J., Cai, Y., Zhang, Y., et al.** (2016). Mitogen-Activated Protein Kinase Cascade MKK7-
911 MPK6 Plays Important Roles in Plant Development and Regulates Shoot
912 Branching by Phosphorylating PIN1 in Arabidopsis. *PLoS Biol* **14**, e1002550.

913 **Jönsson, H., Heisler, M. G., Shapiro, B. E., Meyerowitz, E. M. and Mjolsness, E.** (2006). An auxin-driven polarized transport model for phyllotaxis. *Proc Natl*
915 *Acad Sci USA* **103**, 1633–1638.

916 **Kierzkowski, D., Lenhard, M., Smith, R. S. and Kuhlemeier, C.** (2013).
917 Interaction between meristem tissue layers controls phyllotaxis. *Dev Cell* **26**,
918 616–628.

919 **Kleine-Vehn, J., Dhonukshe, P., Sauer, M., Brewer, P. B., Wisniewska, J., Paciorek, T., Benková, E. and Friml, J.** (2008a). ARF GEF-dependent
921 transcytosis and polar delivery of PIN auxin carriers in Arabidopsis. *Curr Biol*
922 **18**, 526–531.

Kleine-Vehn, J., Leitner, J., Zwiewka, M., Sauer, M., Abas, L., Luschnig, C. and Friml, J. (2008b). Differential degradation of PIN2 auxin efflux carrier by retromer-dependent vacuolar targeting. *Proc Natl Acad Sci USA* **105**, 17812–17817.

Knöller, A. S., Blakeslee, J. J., Richards, E. L., Peer, W. A. and Murphy, A. S. (2010). Brachytic2/ZmABCB1 functions in IAA export from intercalary meristems. *J Exp Bot* **61**, 3689–3696.

Lenhard, M. and Laux, T. (2003). Stem cell homeostasis in the Arabidopsis shoot meristem is regulated by intercellular movement of CLAVATA3 and its sequestration by CLAVATA1. *Development* **130**, 3163–3173.

Leyser, H. M. O. (2005). Auxin Distribution and Plant Pattern Formation: How Many Angels Can Dance on the Point of PIN? *Cell* **121**, 819–822.

Leyser, H. M. O. (2006). Dynamic integration of auxin transport and signalling. *CURBIO* **16**, R424–33.

Leyser, H. M. O. (2010). The power of auxin in plants. *Plant Physiol* **154**, 501–505.

Luschnig, C. and Vert, G. (2014). The dynamics of plant plasma membrane proteins: PINs and beyond. *Development* **141**, 2924–2938.

Martinez, C. C., Koenig, D., Chitwood, D. H. and Sinha, N. R. (2016). A sister of PIN1 gene in tomato (Solanum lycopersicum) defines leaf and flower organ initiation patterns by maintaining epidermal auxin flux. *Dev Biol* **419**, 85–98.

Miao, J., Guo, D., Zhang, J., Huang, Q., Qin, G., Zhang, X., Wan, J., Gu, H. and Qu, L.-J. (2013). Targeted mutagenesis in rice using CRISPR-Cas system. *Cell Res* **23**, 1233–1236.

Mitchison, G. J. (1980). A Model for Vein Formation in Higher Plants. *Proc. Biol. Sci.* **207**, 79–109.

Mitchison, G. J., Hanke, D. E. and Sheldrake, A. R. (1981). The Polar Transport of Auxin and Vein Patterns in Plants [and Discussion]. *Philosophical Transactions of the Royal Society B: Biological Sciences* **295**, 461–471.

Moore, I., Gälweiler, L., Grosskopf, D. and Palme, K. (1998). A transcription activation system for regulated gene expression in transgenic plants. *Proc. Natl. Acad. Sci. U.S.A.* **95**, 376–381.

Multani, D. S., Briggs, S. P., Chamberlin, M. A., Blakeslee, J. J., Murphy, A. S. and Johal, G. S. (2003). Loss of an MDR transporter in compact stalks of maize br2 and sorghum dw3 mutants. *Science* **302**, 81–84.

O'Connor, D. L., Runions, A., Sluis, A., Bragg, J., Vogel, J. P., Prusinkiewicz, P. and Hake, S. (2014). A division in PIN-mediated auxin patterning during organ initiation in grasses. *PLoS Comput Biol* **10**, e1003447.

Okada, K., Ueda, J., Komaki, M. K., Bell, C. J. and Shimura, Y. (1991). Requirement of the Auxin Polar Transport System in Early Stages of Arabidopsis Floral Bud Formation. *The Plant Cell* **3**, 677–684.

Paponov, I. A., Teale, W. D. and Trebar, M. (2005). The PIN auxin efflux facilitators: evolutionary and functional perspectives. *Trends Plant Sci* **10**, 170–177.

Prusinkiewicz, P., Crawford, S., Smith, R. S., Ljung, K., Bennett, T. A., Ongaro, V. and Leyser, H. M. O. (2009). Control of bud activation by an auxin transport switch. *Proc Natl Acad Sci USA* **106**, 17431–17436.

Raven, J. A. (1975). Transport of indoleacetic acid in plant cells in relation to pH and electrical potential gradients, and its significance for polar IAA transport. *New Phytol* **74**, 163–172.

Reinhardt, D., Mandel, T. and Kuhlemeier, C. (2000). Auxin Regulates the Initiation and Radial Position of Plant Lateral Organs. *The Plant Cell* **12**, 507.

Reinhardt, D., Pesce, E.-R., Stieger, P., Mandel, T., Baltensperger, K., Bennett, M. J., Traas, J., Friml, J. and Kuhlemeier, C. (2003). Regulation of phyllotaxis by polar auxin transport. *Nature* **426**, 255–260.

Rubery, P. H. and Sheldrake, A. R. (1974). Carrier-mediated auxin transport. *Planta* **118**, 101–121.

Sauer, M., Balla, J., Luschnig, C., Wisniewska, J., Reinöhl, V., Friml, J. and Benková, E. (2006). Canalization of auxin flow by Aux/IAA-ARF-dependent feedback regulation of PIN polarity. *Genes Dev* **20**, 2902–2911.

Sawchuk, M. G., Edgar, A. and Scarpella, E. (2013). Patterning of Leaf Vein Networks by Convergent Auxin Transport Pathways. *PLoS Genet* **9**, e1003294.

Scarpella, E., Marcos, D., Friml, J. and Berleth, T. (2006). Control of leaf vascular patterning by polar auxin transport. *Genes Dev* **20**, 1015–1027.

Sessions, A., Weigel, D. and Yanofsky, M. F. (2002). The Arabidopsis thaliana MERISTEM LAYER 1 promoter specifies epidermal expression in meristems and young primordia. *Plant J* **20**, 259–263.

Shinohara, N., Taylor, C. and Leyser, H. M. O. (2013). Strigolactone Can Promote or Inhibit Shoot Branching by Triggering Rapid Depletion of the Auxin Efflux Protein PIN1 from the Plasma Membrane. *PLoS Biol* **11**, e1001474.

Smith, R. S., Guyomarc'h, S., Mandel, T., Reinhardt, D., Kuhlemeier, C. and Prusinkiewicz, P. (2006). A plausible model of phyllotaxis. *Proc. Natl. Acad. Sci. U.S.A.* **103**, 1301–1306.

Stoma, S., Lucas, M., Chopard, J., Schaedel, M. and Godin, C. (2008). Flux-Based Transport Enhancement as a Plausible Unifying Mechanism for Auxin Transport in Meristem Development. *PLoS Comput Biol* **4**, e1000207.

Torii, K. U., Mitsukawa, N., Oosumi, T., Matsuura, Y., Yokoyama, R., Whittier, R. F. and Komeda, Y. (1996). The Arabidopsis ERECTA gene encodes a putative receptor protein kinase with extracellular leucine-rich repeats. *The Plant Cell* **8**, 735–746.

Verna, C., Sawchuk, M. G., Linh, N. M. and Scarpella, E. (2015). Control of vein network topology by auxin transport. *BMC Biol* **13**, 94.

Vieten, A., Vanneste, S., Wisniewska, J., Benkova, E., Benjamins, R., Beeckman, T., Luschnig, C. and Friml, J. (2005). Functional redundancy of PIN proteins is accompanied by auxin-dependent cross-regulation of PIN expression. *Development* **132**, 4521–4531.

Wang, R. and Estelle, M. (2014). Diversity and specificity: auxin perception and signaling through the TIR1/AFB pathway. *Curr Opin Plant Biol* **21**, 51–58.

Weller, B., Zourelidou, M., Frank, L., Barbosa, I. C. R., Fastner, A., Richter, S., Jürgens, G., Hammes, U. Z. and Schwechheimer, C. (2017). Dynamic PIN-FORMED auxin efflux carrier phosphorylation at the plasma membrane controls auxin efflux-dependent growth. *Proc Natl Acad Sci USA* **114**, E887–E896.

Willige, B. C., Ahlers, S., Zourelidou, M., Barbosa, I. C. R., Demarsy, E., Trevisan, M., Davis, P. A., Roelfsema, M. R. G., Hangarter, R., Fankhauser, C., et al. (2013). D6PK AGCVIII kinases are required for auxin transport and phototropic hypocotyl bending in Arabidopsis. *The Plant Cell* **25**, 1674–1688.

Wisniewska, J., Xu, J., Seifertová, D., Brewer, P. B., Ruzicka, K., Blilou, I., Rouquié, D., Benková, E., Scheres, B. and Friml, J. (2006). Polar PIN localization directs auxin flow in plants. *Science* **312**, 883–883.

Xu, J., Hofhuis, H., Heidstra, R., Sauer, M., Friml, J. and Scheres, B. (2006). A molecular framework for plant regeneration. *Science* **311**, 385–388.

Zhou, C., Han, L., Hou, C., Metelli, A., Qi, L., Tadege, M., Mysore, K. S. and Wang, Z.-Y. (2011). Developmental analysis of a Medicago truncatula smooth leaf margin1 mutant reveals context-dependent effects on compound leaf development. *The Plant Cell* **23**, 2106–2124.

Figures and Legends

Figure 1. Mutation of SoPIN1 but not PIN1a and PIN1b severely effects organ initiation in Brachypodium. (A) *SoPIN1*, *PIN1a*, and *PIN1b* CRISPR-derived mutant alleles (see methods). Coding sequences are indicated by grey boxes. Arrowheads indicate CRISPR target sites and are labeled with the type of DNA lesion (C insertion, T insertion, or A deletion). All mutant alleles have frame shifts that result in premature stop codons at the positions indicated. **(B-G)** Inflorescence phenotypes of CRISPR-derived *sopin1-1, pin1a-1*, and *pin1b-1* mutants. See Figure 2 for whole-plant phenotypes. **(B-E)** and **(G)** are scanning electron microscopy (SEM). **(B)** Immature wild-type (WT) (inbred line Bd21-3) Brachypodium inflorescence with several lateral spikelet meristems (lsm), and a terminal spikelet meristem (tsm). **(C)** *sopin1-1* plants have severe organ initiation defects in the inflorescence. **(D)** Detail of a wild-type lateral spikelet meristem outlined by a box in **(B)** showing an immature lemma (l), which is the leaf-like organ that subtends the floral meristem (fm). **(E)** Detail of barren lateral spikelet meristem outlined by box in **(C). (F)** Mature inflorescence phenotypes of WT (Inbred Bd21-3), *sopin1-1, pin1a-1, pin1b-1,* and double *pin1a-1 / pin1b-1* mutants. The terminal spikelet (ts) of each inflorescence is indicated for comparison. Arrowhead indicates bent internode tissue in *pin1b-1.* Genotypes for **(G-I)** are indicated at the bottom of **(I). (G)** SEM details of representative spikelet meristems**. (H)** Box-plot of total whole-plant spikelet number at seed-set. (n = 22-53 plants each genotype). Samples with different letters are significantly different from each other (ANOVA, Tukey HSD, $p < 0.05$). See "Figure 1 H-I Source Data 1" for source data. **(I)** Box-plot of the number of florets in each terminal spikelet of the central branch at seed set. (n = 22-53 plants each

genotype). Samples with different letters are significantly different from each other (ANOVA, Tukey HSD, $p < 0.05$). See "Figure 1 H-I Source Data 1" for source data. **(J)** Medial confocal Z-section of pZmUbi::DII-Venus (DII) expression in a WT spikelet co-expressing SoPIN1 tagged with Cerulean (a CFP variant) under the native *SoPIN1* promoter. Organ primordia are numbered I2, I1, P1 from youngest to oldest. DII is normally degraded at SoPIN1 convergence points in I2 and I1 primordia (asterisks), and in response to auxin treatment (See Figure 1 – supplement 2). Inset shows color look-up-table for all subsequent PIN images and color look-up-table for DII. **(K)** Medial confocal Z-section of pZmUbi::DII-Venus expression in a *sopin1-1* spikelet meristem. DII degradation does not occur in the periphery of *sopin1-1* meristems, and organs fail to initiate (arrow). Scale bars: 100μm in **(B)** and **(C)**, 20μm in **(D)** and **(E),** 1cm in **(F),** 50μm each in **(G),** and 25μm in **(J)** and **(K).**

Figure 1 – supplement 1. *sopin1-1* is complemented by the SoPIN1-CIT reporter. **(A)** Wild-type inflorescence (Bd21-3 background) with wild-type mature spikelets (s). **(B)** *sopin1-1* inflorescence with an aborted spikelet (asterisk) and several barren white spikelet nodes (n). Green internode (i) tissue is also labeled. **(C)** Inflorescence of a *sopin1-1* mutant plant complemented by previously published full-length SoPIN1 internal CITRINE fluorescent protein fusion under the native *SoPIN1* promoter (+SoPIN1-CIT) (O'Connor et al., 2014). Scale bars: 1cm.

Figure 1 – supplement 2. DII-Venus is degraded in the presence of auxin in Brachypodium spikelet meristems. **(A)** 1 μM NAA-treated, and **(B)** mock-treated

spikelet meristems expressing pZmUbi::DII-Venus imaged every 30 min after treatment. Images from left to right, pre-treatment expression, 30 min, 60 min and 90 min time-points. **(C)** Relative mean fluorescence in a radius at the spikelet meristem tip in NAA-treated and Mock samples at 0, 30, 60 and 90-minute time points. Scale bars: 25μm.

Figure 1 - Source Data 1. Source data for spikelet and floret counts in Figure 1 H-I.

Figure 1 – Source Data 2. Source data for DII quantification in Figure 1 – supplement 2 panel C.

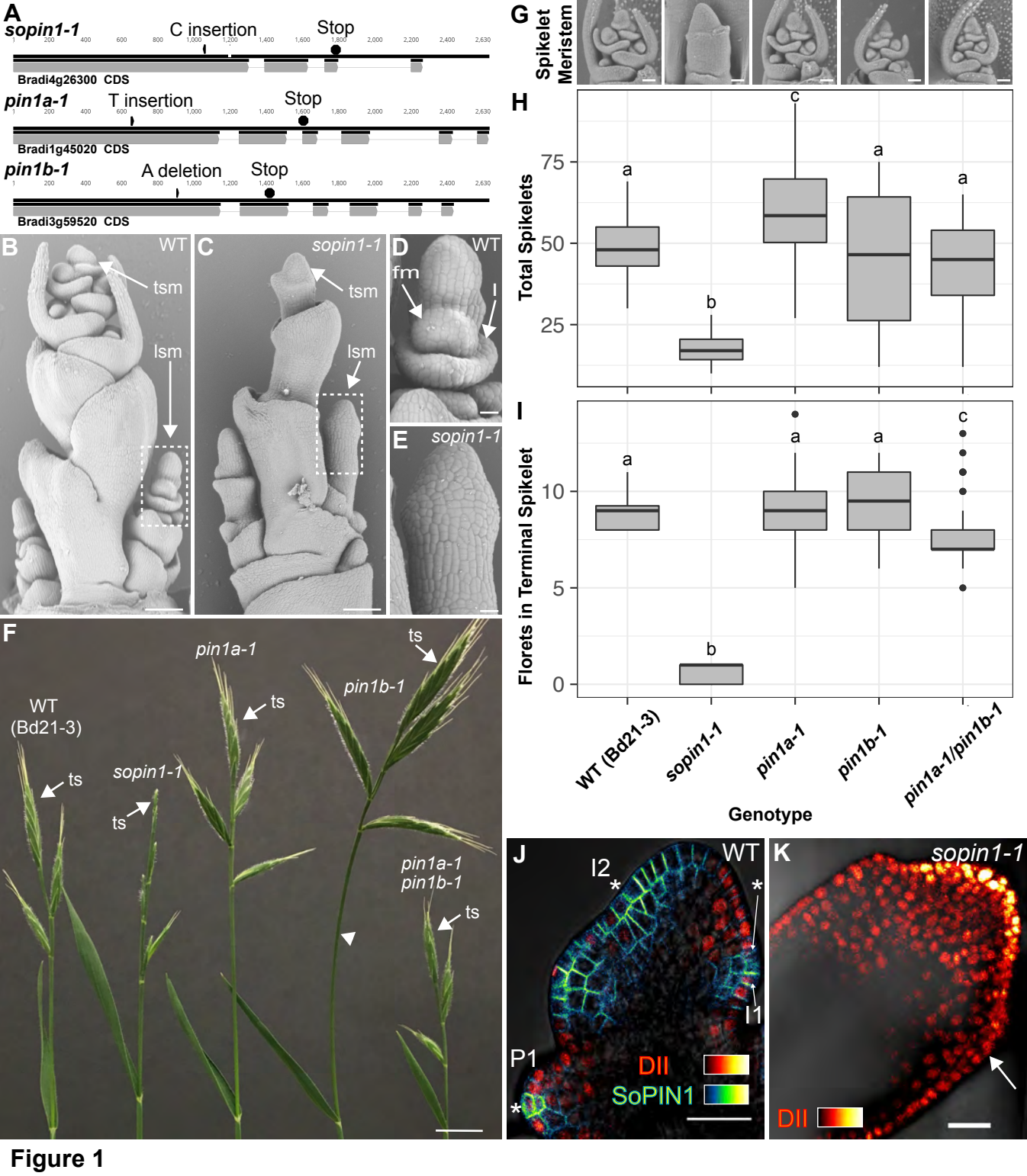
A
sopin1-1
C insertion
Stop
Bradi4g26300 CDS
pin1a-1
T insertion
Stop
Bradi1g45020 CDS
pin1b-1
A deletion
Stop
Bradi3g59520 CDS
B
WT
tsm
lsm
C
sopin1-1
tsm
lsm
D
WT
fm
l
E
sopin1-1
F
WT
(Bd21-3)
ts
sopin1-1
ts
pin1a-1
ts
pin1b-1
ts
pin1a-1
pin1b-1
ts
G
Spikelet
Meristem
H
Total Spikelets
75
50
25
a
b
c
a
a
I
Florets in Terminal Spikelet
10
5
0
a
b
a
a
c
WT (Bd21-3)
sopin1-1
pin1a-1
pin1b-1
pin1a-1/pin1b-1
Genotype
J
WT
I2
I1
P1
DII
SoPIN1
K
sopin1-1
DII

Figure 1

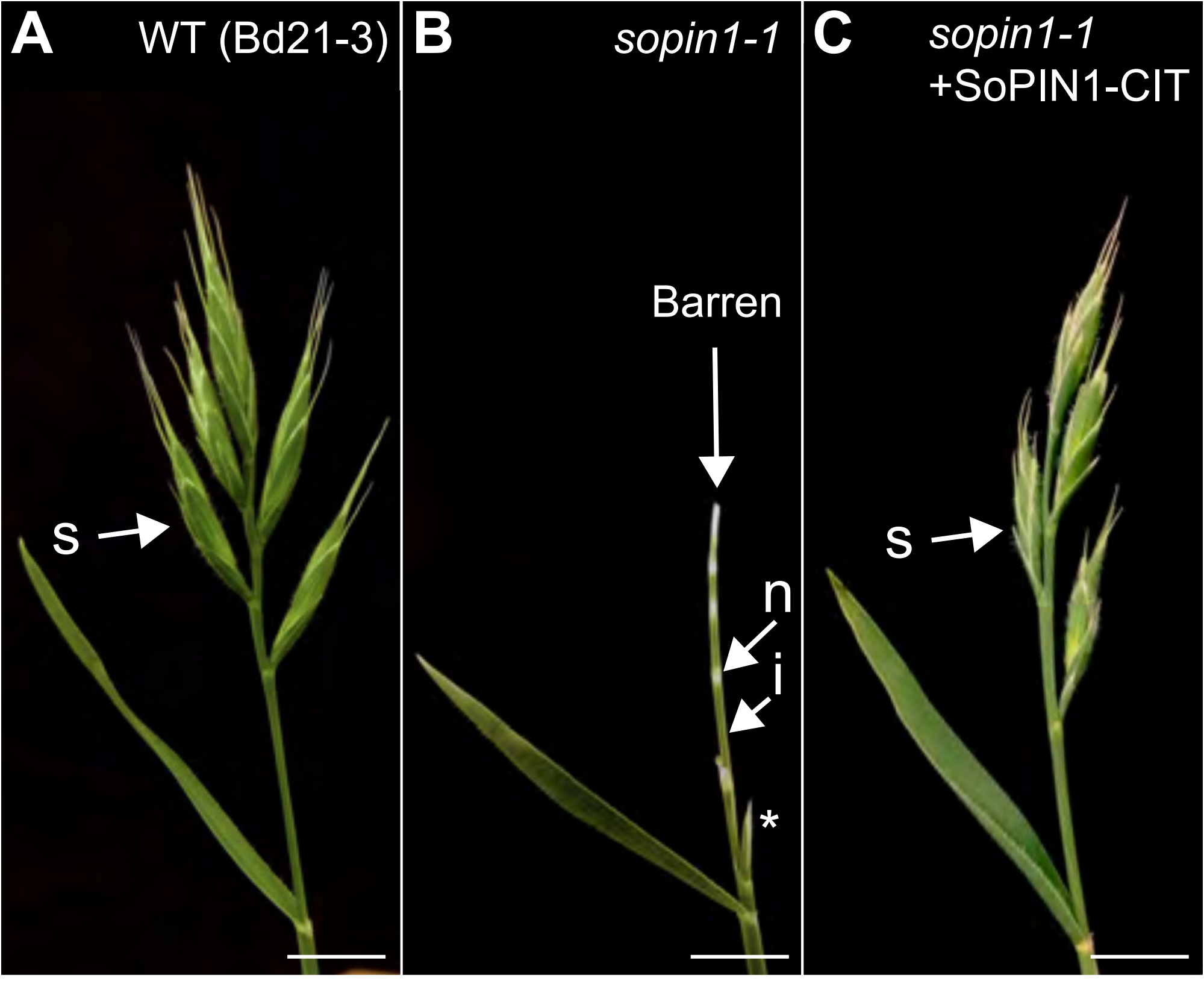

Figure 1 - supplement 1

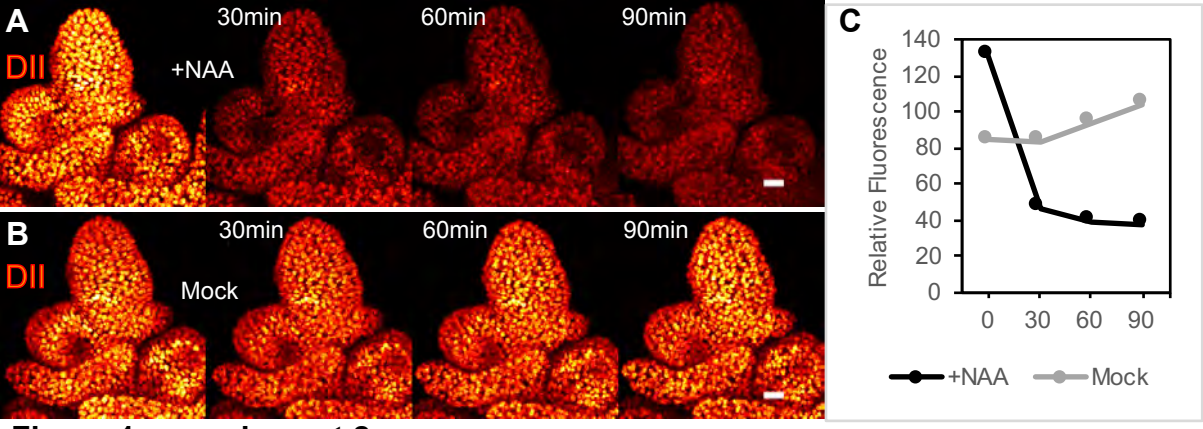

Figure 1 - supplement 2

Figure 2 - PIN1a and PIN1b redundantly control internode growth in Brachypodium. (A-D) Whole-plant phenotypes for WT (Bd21-3), *pin1a-1*, *pin1b-1*, and double *pin1a-1 / pin1b-1* mutants. **(E)** Stacked bar graph of the length of the first 5 internodes below the inflorescence of the main branch, labeled I1-I5 from top to bottom. Lines connect analogous internodes between genotypes. Analogous internodes with different letters are significantly different from each other (ANOVA, Tukey HSD, $p < 0.05$). I5 internodes were not significantly different between genotypes and are unlabeled. Internode lengths significantly different from WT are indicated by asterisks. (n = 18-51 individuals each genotype) See "Figure 2 Source Data 1" for source data. Scale bars: 1cm in **(A-D)**.

Figure 2 – supplement 1. PIN1b-CIT-mediated complementation of *pin1b-1* internode length defects. Stacked bar graph of the length of the first 5 internodes below the inflorescence of the main branch, labeled I1-I5 from top to bottom, for *pin1b-1* and *pin1b-1* containing the previously published full-length PIN1b internal CITRINE fluorescent protein fusion under the native *PIN1b* promoter (+PIN1b-CIT) (O'Connor et al., 2014) (n = 10 each genotype). Lines connect analogous internodes between genotypes. Internodes that are significantly different between genotypes are marked with asterisks. The I4 and I5 internodes are significantly shorter in the complemented line than in *pin1b-1* (ANOVA, Tukey HSD, $p < 0.05$). See "Figure 2 Source Data 2" for source data.

Figure 2 Source Data 1. Source data for internode length measurements in Figure 2E.

Figure 2 Source Data 2. Source data for PIN1b-CIT-mediated complementation of *pin1b-1* internode lengths in Figure 2 - supplement 1.

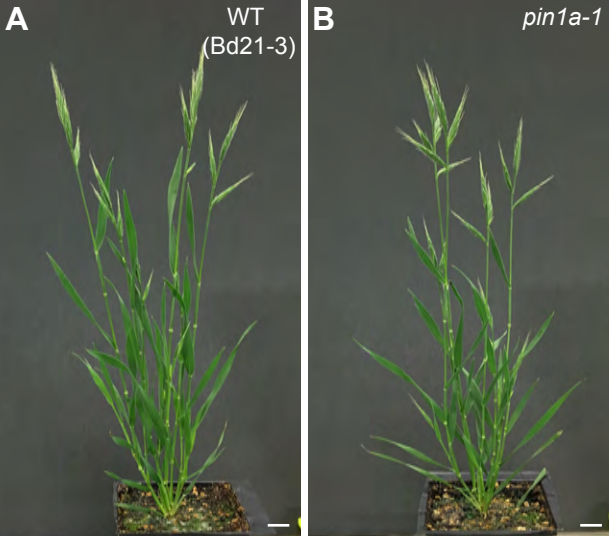
A
WT
(Bd21-3)

B
pin1a-1


C
pin1b-1

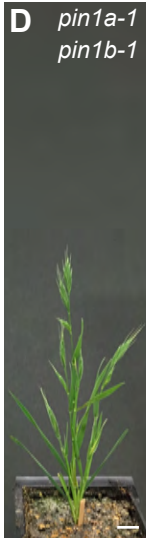
D
pin1a-1
pin1b-1

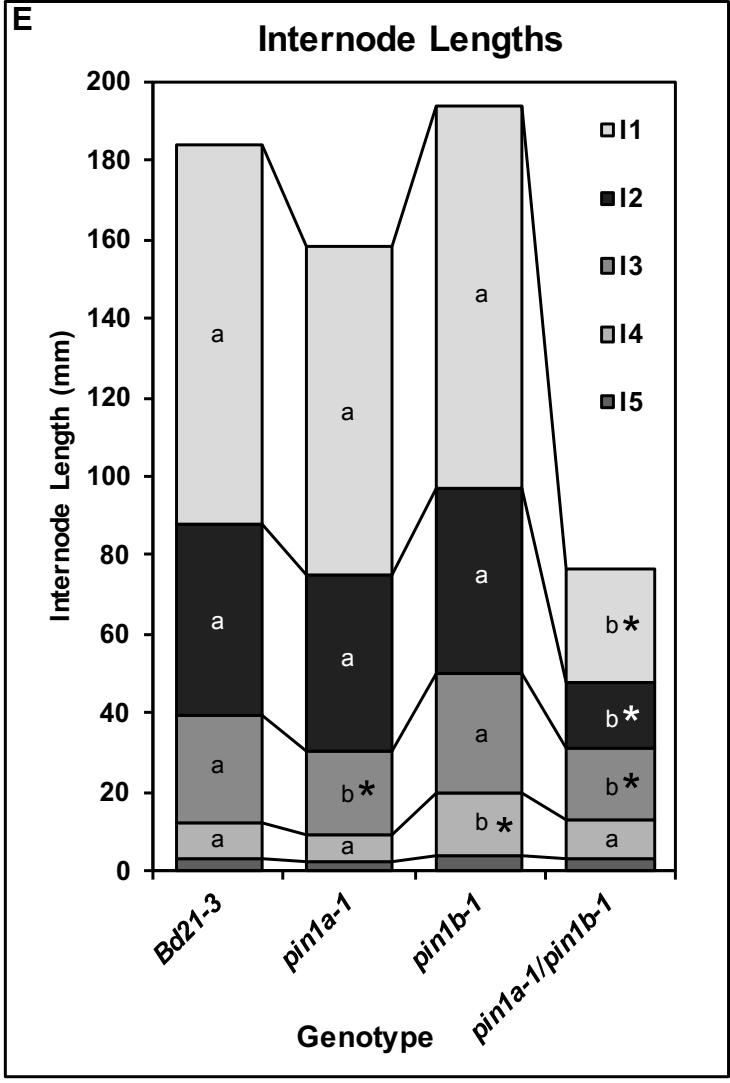
E
Internode Lengths
Internode Length (mm)
200
180
160
140
120
100
80
60
40
20
0
I1
I2
I3
I4
I5
a
a
a
a
a
a
a
a
a
a
b*
b*
b*
b*
b*
Bd21-3
pin1a-1
pin1b-1
pin1a-1/pin1b-1
Genotype

Figure 2

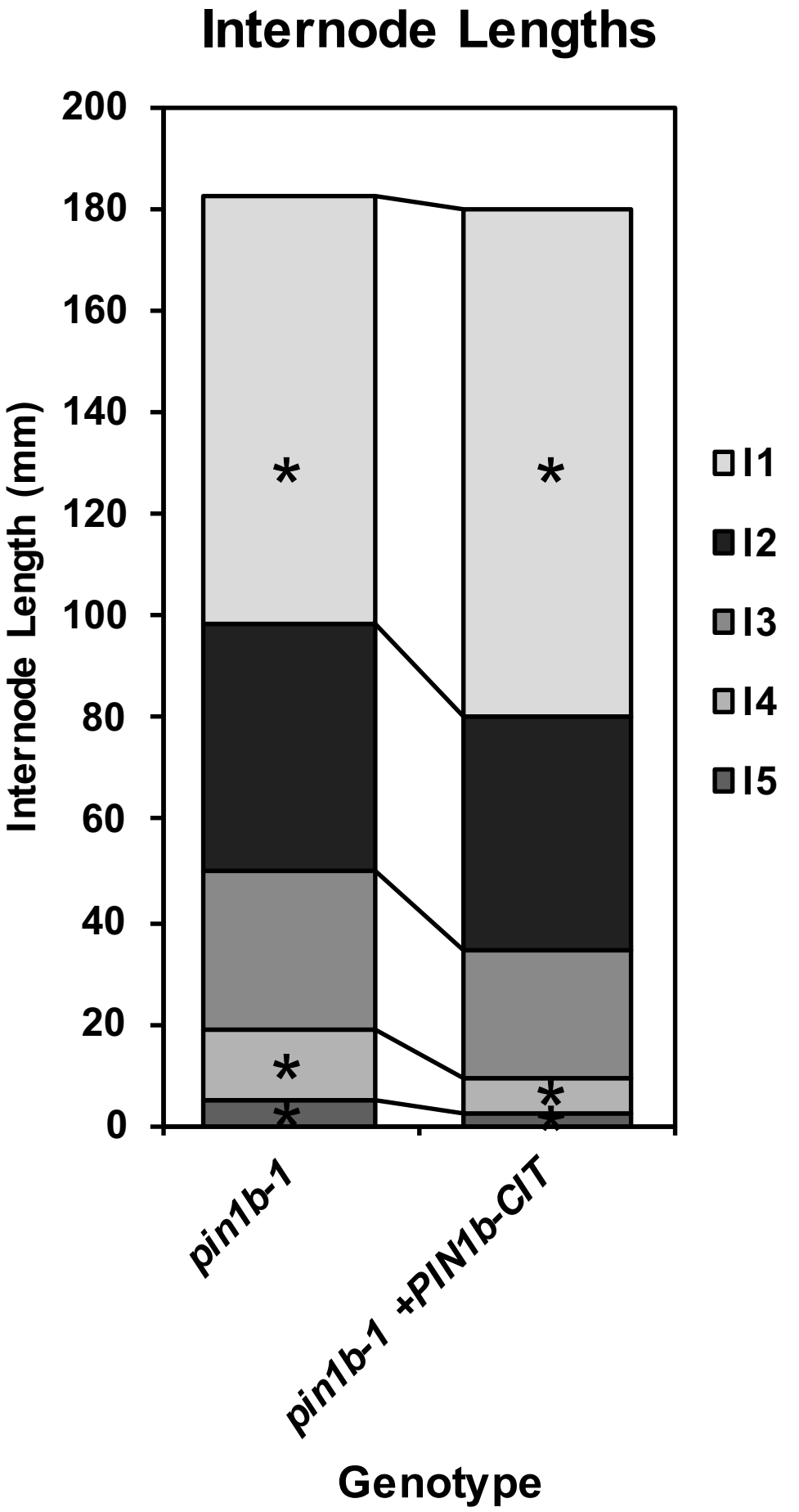

Figure 2 - supplement 1

Figure 3. AtPIN1, SoPIN1, and PIN1b show different behaviors when expressed in wild-type Arabidopsis. Arabidopsis *AtPIN1* promoter (*proAtPIN1*) driven expression of GFP-tagged AtPIN1 and CITRINE-tagged (a YFP derivative) SoPIN1 and PIN1b in wild-type Columbia (Col-0) Arabidopsis. **(A,D,G,J)** AtPIN1, **(B,E,H,K)** SoPIN1, **(C,F,I,L)** PIN1b. **(A-C)** Maximum projections of meristem apexes. Arrows in (**A)** and **(B)** indicate convergence points (cp) in I2 primordium. Arrowhead in **(C)** indicates internalized PIN1b in punctate membrane bodies. The I2 and I1 primordia are labeled. **(D-F)** Tiled confocal maximum projections of longitudinal hand-sections through inflorescence apexes. Arrows indicate SoPIN1 epidermal expression in sepal primordia and flower pedicels in **(E)** and the lack of AtPIN1 and PIN1b epidermal expression in the same tissues in **(D)** and **(F)**. Box in **(D)** shows detail area in Figure 3 – supplement 1 panel D**. (G-I)** Tiled confocal maximum projections of longitudinal hand-sections through basal inflorescence stem internodes 1cm above the rosette. **(J-L)** Tiled confocal maximum projections of hand cross-sections through basal internodes 1cm above the rosette. Signal at the edge of each section (arrowheads) is cuticle auto-florescence. The cortex (co), cambium (ca), xylem parenchyma (xp), and pith (p) tissues are indicated in **(G-L)**. Arrows in **(H)** and **(K)** indicate cortex and pith ectopic expression of SoPIN1. Red signal in all panels is chlorophyll auto-florescence. Scale bars: 25μm in **(A-C)**, and 100μm in **(D-L)**.

Figure 3 – supplement 1. *proAtPIN1* AtPIN1, SoPIN1, and PIN1b expression details. (A) Confocal z-section of AtPIN1 accumulation in vascular-associated domains just below the apex of the meristem shown in Figure 3A. **(B)** Confocal z-section of SoPIN1 accumulation in a ring-shaped domain just below the apex of the meristem

shown in Figure 3B. **(C)** Confocal z-section of PIN1b accumulation in vascular-associated domains just below the apex of the meristem shown in Figure 3C. (**D)** Maximum projection detail of AtPIN1 accumulation in both pith (p) and procambium (pc) tissues in the immature inflorescence stem outlined with a box in Figure 3D. **(E)** Maximum projection detail of rootward polarized SoPIN1 (arrows) in a longitudinal hand-section of the basal internode pith tissue. **(F)** Maximum projection detail of rootward polarized PIN1b (arrows) in a longitudinal hand-section of the basal internode xylem parenchyma tissue. Red signal in **(D-F)** is chlorophyll auto-florescence. Scale bars: 25µm.

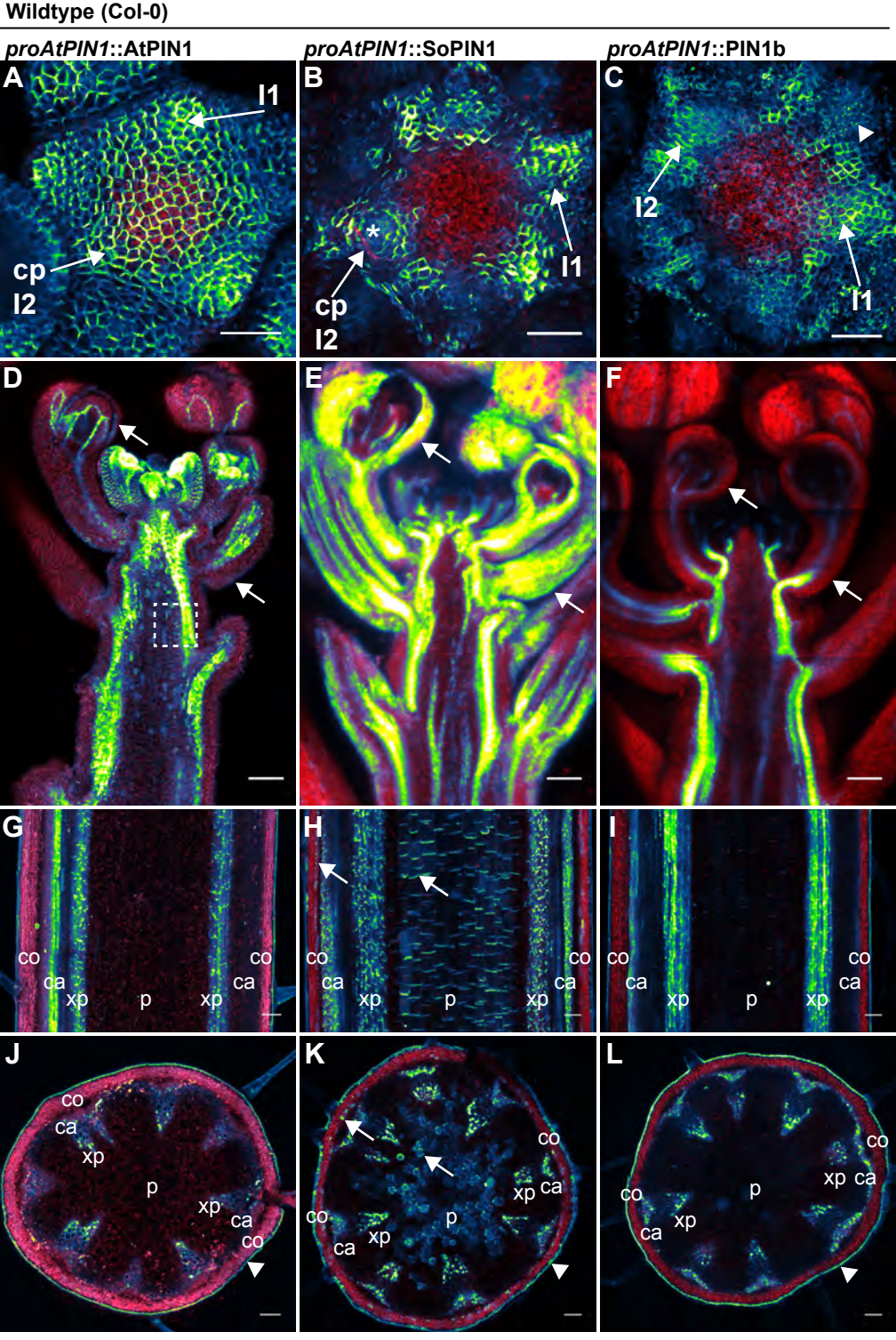
Wildtype (Col-0)
proAtPIN1::AtPIN1
proAtPIN1::SoPIN1
proAtPIN1::PIN1b
A
I1
cp
I2
B
*
I1
cp
I2
C
I2
I1
D
E
F
G
co
ca
xp
p
xp
ca
co
H
co
ca
xp
p
xp
ca
co
I
co
ca
xp
p
xp
ca
co
J
co
ca
xp
p
xp
ca
co
K
co
xp
ca
co
ca
xp
p
L
co
xp
ca
co
p
ca
xp

Figure 3

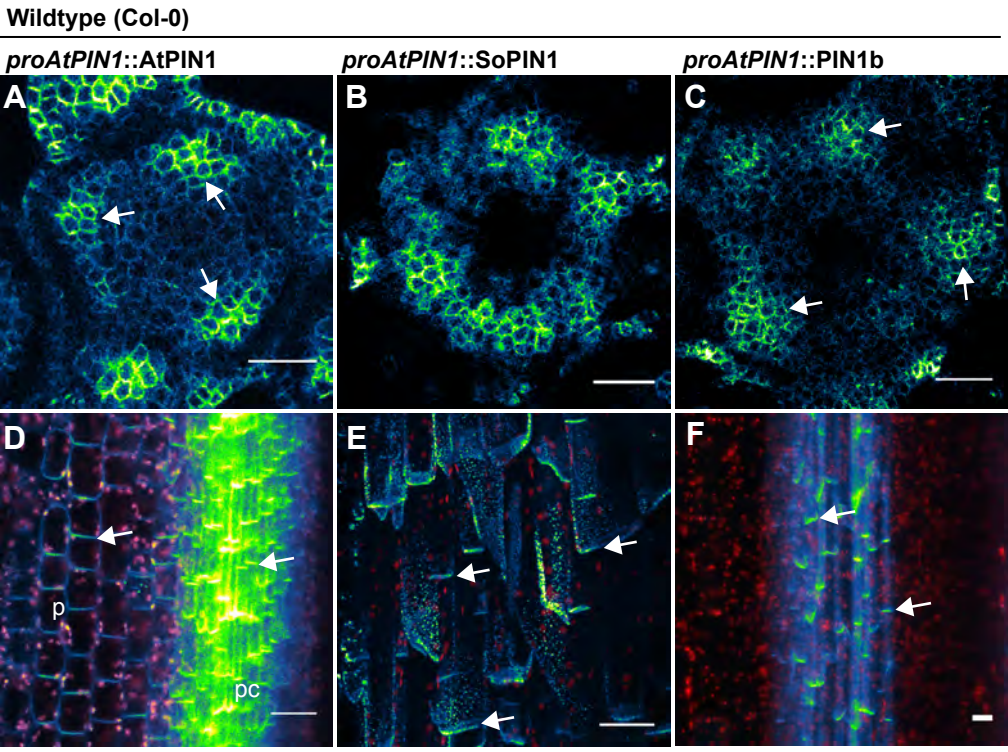

Figure 3 - supplement 1

Figure 4. SoPIN1 but not PIN1b can partially complement the Arabidopsis *pin1-613* mutant organ initiation and bulk transport defects. (A) From left to right, inflorescence phenotypes of WT (Col-0), *proAtPIN1::*SoPIN1 in *pin1-613,* *proAtPIN1*::PIN1b in *pin1-613,* and *pin1-613* alone. Note that PIN1b-expressing *pin1-613* plants are indistinguishable from *pin1-613* alone. See Figure 4 - supplement 1 for whole-plant phenotypes. **(B)** Flower (left), and inflorescence apex (right) of WT (Col-0). **(C)** Flower (left), and inflorescence apex (right) of *proAtPIN1::*SoPIN1 complemented *pin1-613* mutants. Note the increase in petal number and lack of stamens in the flower, see Figure 4 - supplement 2 for organ counts. **(D)** Box-plot of bulk auxin transport (counts per minute, CPM) through basal internodes 1cm above the rosette of 40-day-old Arabidopsis inflorescence stems. (n=16 each genotype). Samples with different letters are significantly different from each other (ANOVA, Tukey HSD, $p < 0.05$). See Figure 3 - Source Data 1 for source data. Scale bars: 1cm in **(A)**, 1mm in **(B-C)**.

Figure 4 - supplement 1. Whole-plant phenotypes of *proAtPIN1*-driven complementation of *pin1-613.* From left to right, Col-0 (WT), *proAtPIN1::*SoPIN1 complemented *pin1-613*, *proAtPIN1::*PIN1b expressing *pin1-613,* and *pin1-613* alone. Scale bar: 1cm.

Figure 4 - supplement 2. Floral organ number in *proAtPIN1::*SoPIN1 complemented flowers. Mean and standard-error of sepal, petal, stamen and carpel organ numbers in heterozygous *pin1-613* or wild-type (white bars), and

*proAtPIN1::*SoPIN1-complemented *pin1-613* flowers (grey bars) (n=30). See Figure 4 - Source Data 2 for source data.

Figure 4 - Source Data 1. Source data for Figure 4D auxin transport assays.

Figure 4 - Source Data 2. Source data for Figure 4 - supplement 2 floral organ numbers.

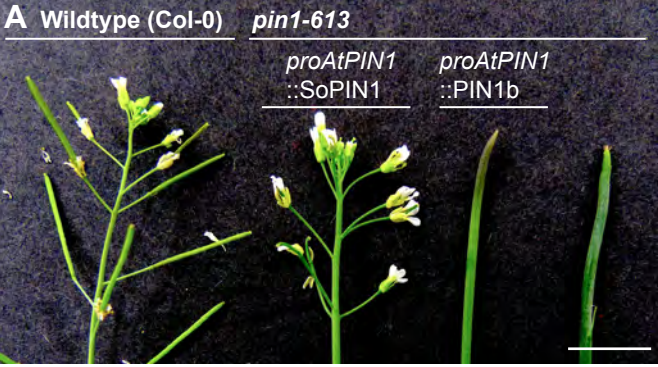
A Wildtype (Col-0)
pin1-613
proAtPIN1 ::SoPIN1
proAtPIN1 ::PIN1b

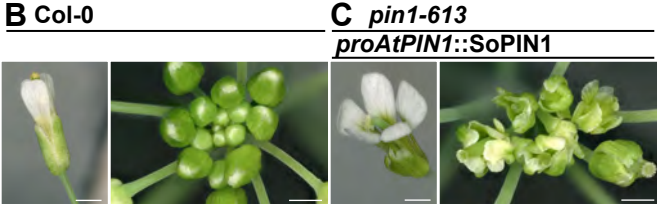
B Col-0
C pin1-613
proAtPIN1::SoPIN1

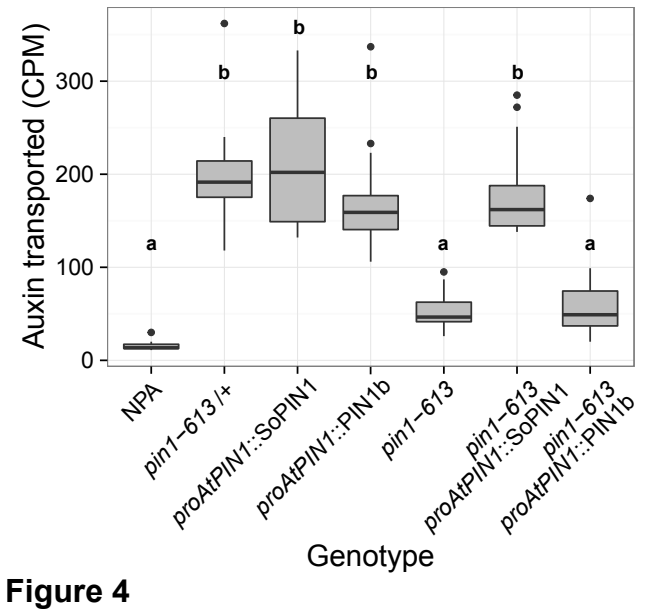
D Stem auxin transport
Auxin transported (CPM)
0
100
200
300
a
b
b
b
a
b
a
NPA
pin1−613/+
proAtPIN1::SoPIN1
proAtPIN1::PIN1b
pin1−613
pin1−613 proAtPIN1::SoPIN1
pin1−613 proAtPIN1::PIN1b
Genotype

Figure 4

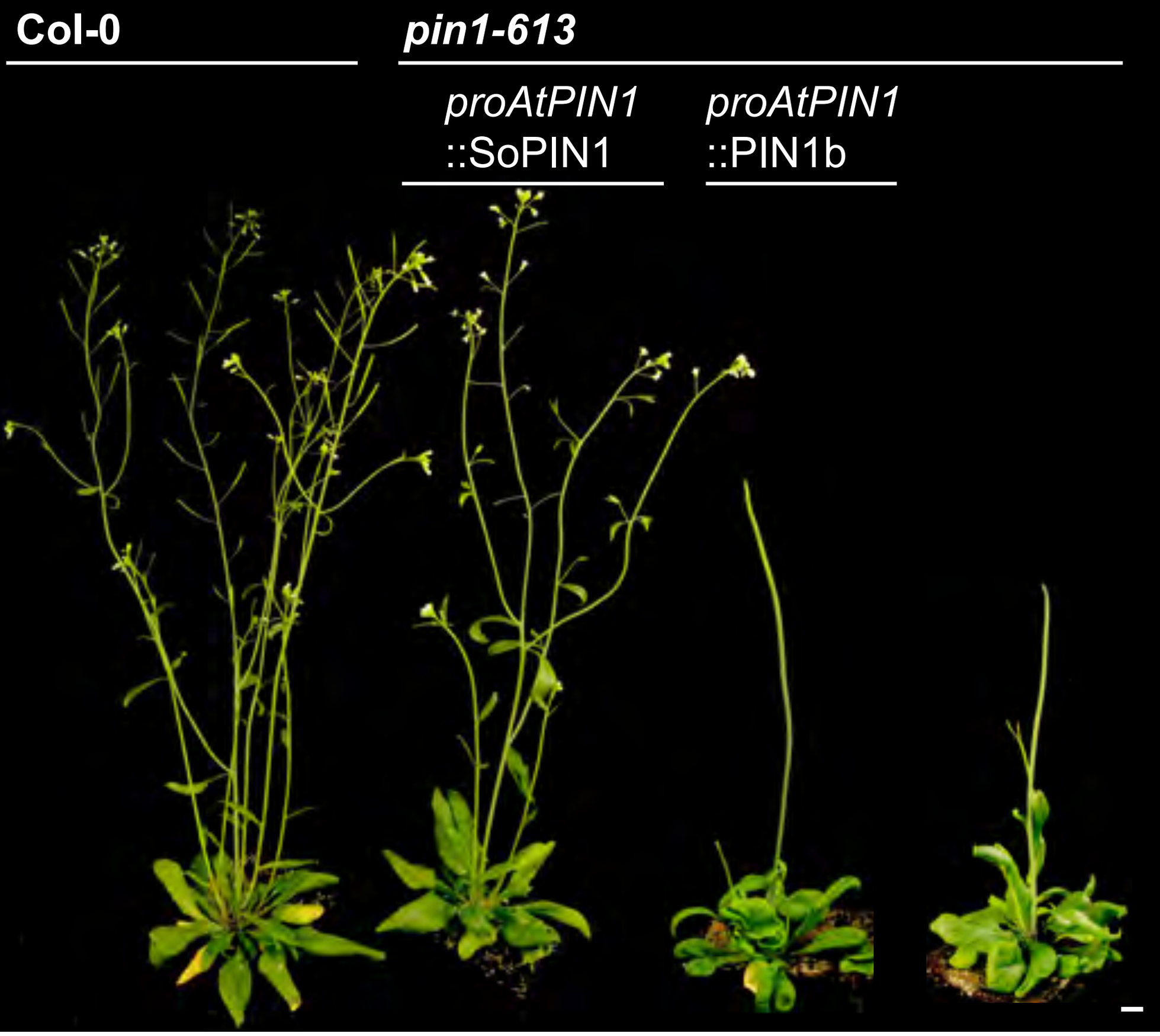

Figure 4 - supplement 1

Floral organ number - *proAtPIN1::*SoPIN1

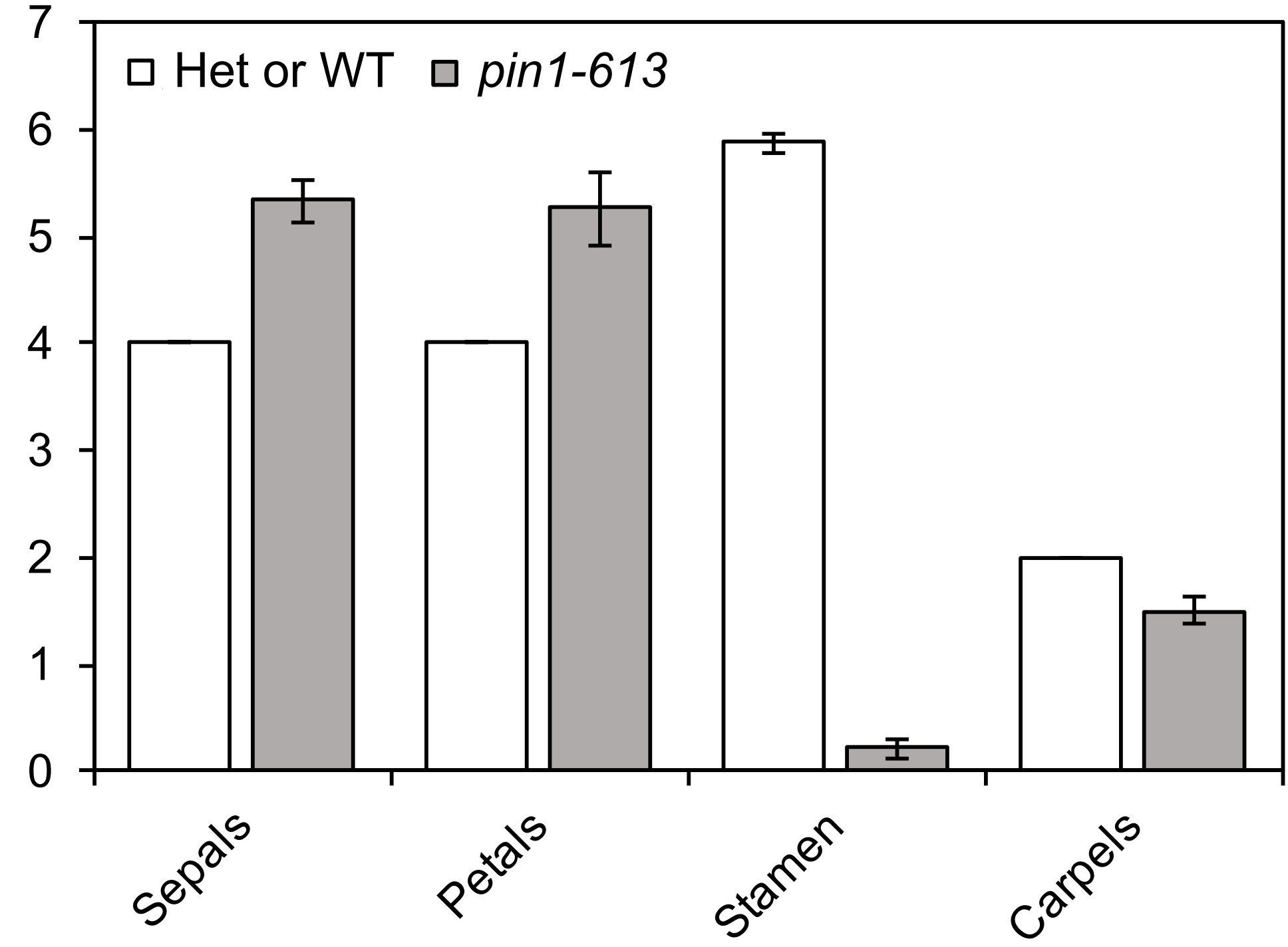

Figure 4 - supplement 2

Figure 5. SoPIN1 and PIN1b localization in null *pin1-613* mutants. Arabidopsis *PIN1* promoter (*proAtPIN1*) driven expression of Citrine-tagged (YFP derivative) SoPIN1 and PIN1b in null *pin1-613* mutant tissue. **(A,C,E,G,I)** SoPIN1, **(B,D,F,H,J,K,L,M)** PIN1b. **(A-B)** Maximum projections of meristem apexes. Arrow in **(B)** indicates PIN1b ring shaped epidermal domain. See Figure 5 – supplement 1 for SoPIN1 expression in a *pin1-613* segregating family. See Figure 5 – supplement 2 for more examples of PIN1b expression in *pin1-613* apexes, and Figure 5 – supplement 3 for PIN1b dynamics in response to auxin addition. **(C-D)** Tiled confocal maximum projections of longitudinal hand-sections through apexes. Arrow in **(D)** indicates increased PIN1b in the epidermis in the *pin1-613* background. **(E-F)** Tiled maximum projections of longitudinal hand-sections through basal inflorescence stem internodes 1cm above the rosette. **(G-H)** Tiled maximum projections of hand cross-sections through basal internodes 1cm above the rosette. Signal at the edge of each section (arrowheads) is cuticle auto-florescence. The cortex (co), cambium (ca), xylem parenchyma (xp), and pith (p) tissues are indicated in **(E-H).** Arrows in **(E)** and **(G)** indicate cortex and pith accumulation of SoPIN1. **(I)** Confocal z-section of SoPIN1 accumulation in a ring-shaped domain just below the apex of a complemented *pin1-613* meristem. **(J)** Longitudinal hand-section of PIN1b just below a *pin1-613* meristem apex. Arrow shows rootward polarized PIN1b. **(K)** Detail of polarized PIN1b in the meristem epidermis of a *pin1-613* meristem apex. **(L)** Cross-section of PIN1b (arrow) in distinct bundles 2mm below a *pin1-613* meristem apex. **(M)** Rootward polarization of PIN1b (arrow) 3-4 mm below the apex of a *pin1-613* meristem. Red signal in all panels is chlorophyll auto-florescence. Scale bars: 25μm in **(A-B),** 100μm in **(C-H),** and 25μm in **(I-M)**.

Figure 5 – supplement 1. *proAtPIN1::*SoPIN1 expression in *pin1-613* segregating family. (A) *proAtPIN1::*SoPIN1 expression in 6 different WT or heterozygous *pin1-613* meristem samples. **(B)** *proAtPIN1::*SoPIN1 expression in 6 different complemented *pin1-613* meristems. All samples were imaged with identical settings to show the increase in SoPIN1 accumulation in the *pin1-613* mutant background. Red signal is chlorophyll auto-florescence. Scale bars: 25µm.

Figure 5 – supplement 2. *proAtPIN1::*PIN1b expression in *pin1-613* apexes. Two representative meristems each from four different transgenic events. All samples were imaged with identical settings. Scale bars: 25µm.

Figure 5 – supplement 3. *proAtPIN1::*PIN1b dynamics during organ formation induced by addition of lanolin containing 1mM IAA on *pin1-613* apexes. From left to right, pre-treatment, 24, 48, 72, and 96 hours after treatment. Four representative samples are shown top to bottom. Arrows indicate the lanolin paste at the 24-hour time-point. All samples were imaged with identical settings. Scale bars 25µm.

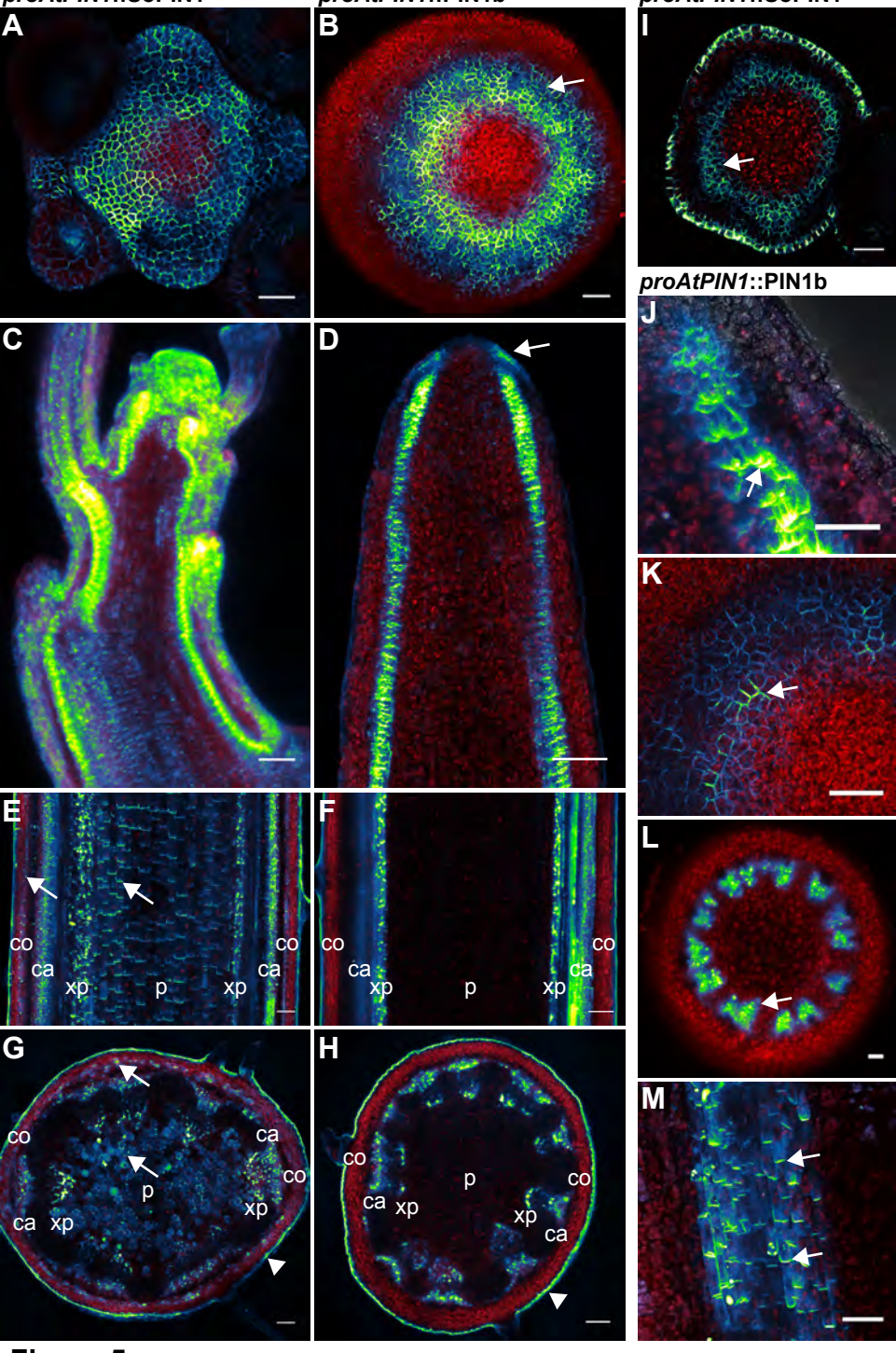
proAtPIN1::SoPIN1
proAtPIN1::PIN1b
proAtPIN1::SoPIN1
proAtPIN1::PIN1b
A
B
I
C
D
J
K
E
F
L
G
H
M
co
ca
xp
p

Figure 5

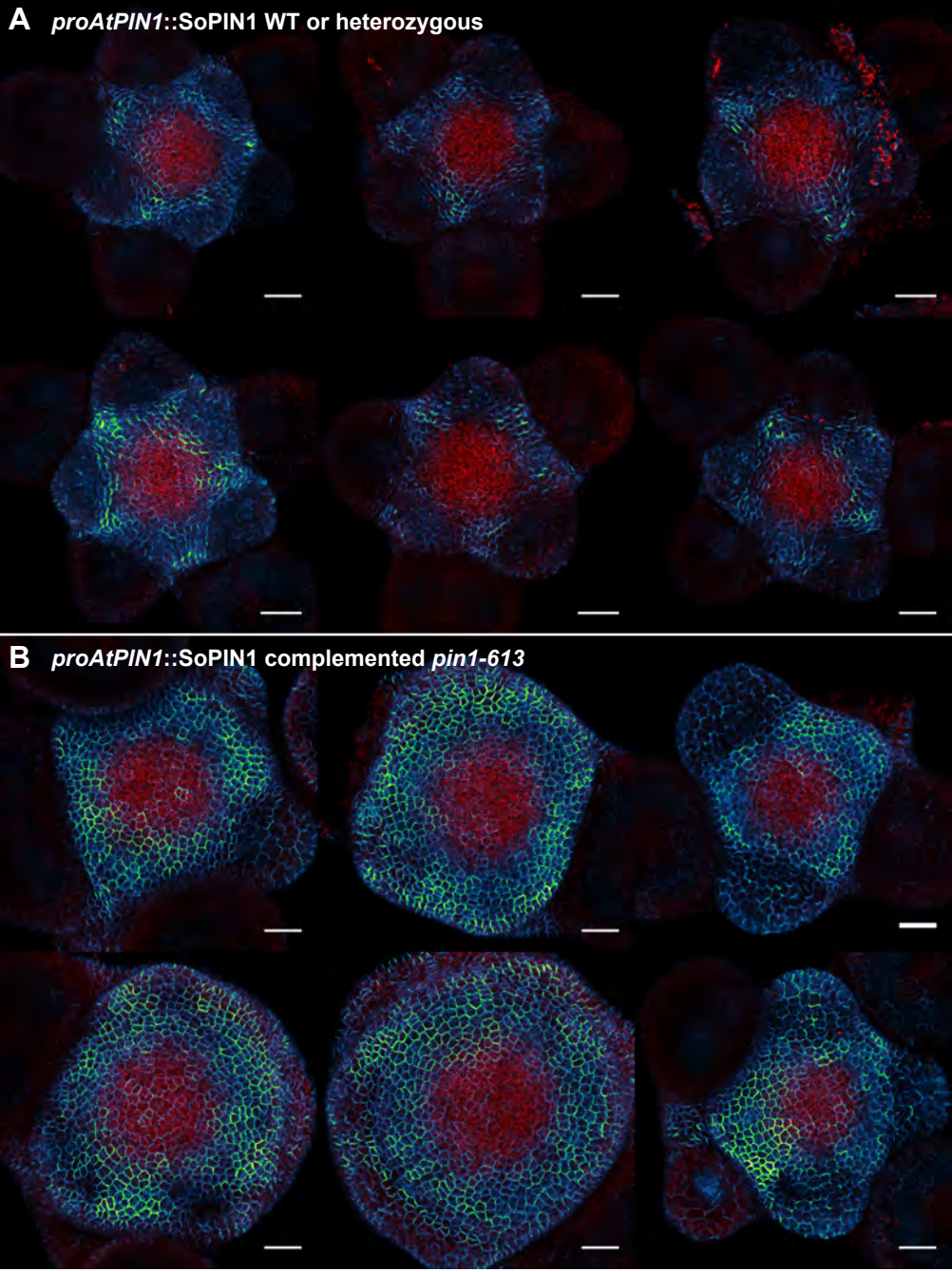

Figure 5 - supplement 1

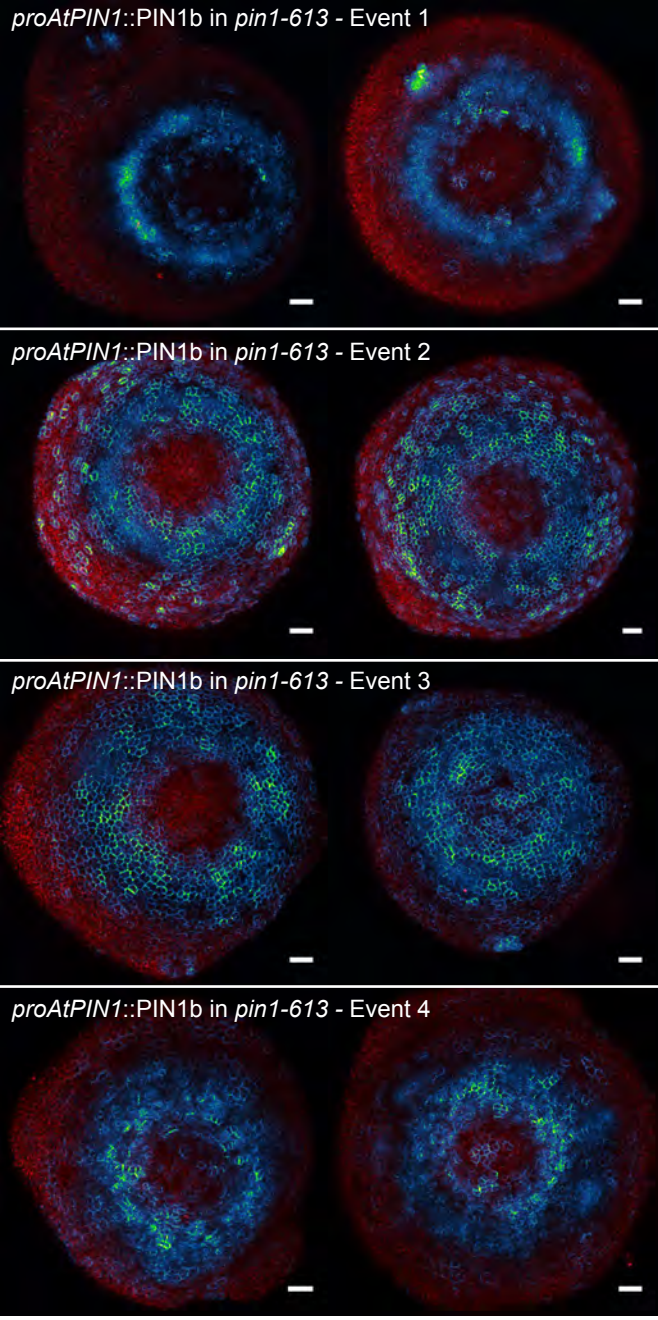

Figure 5 - supplement 2

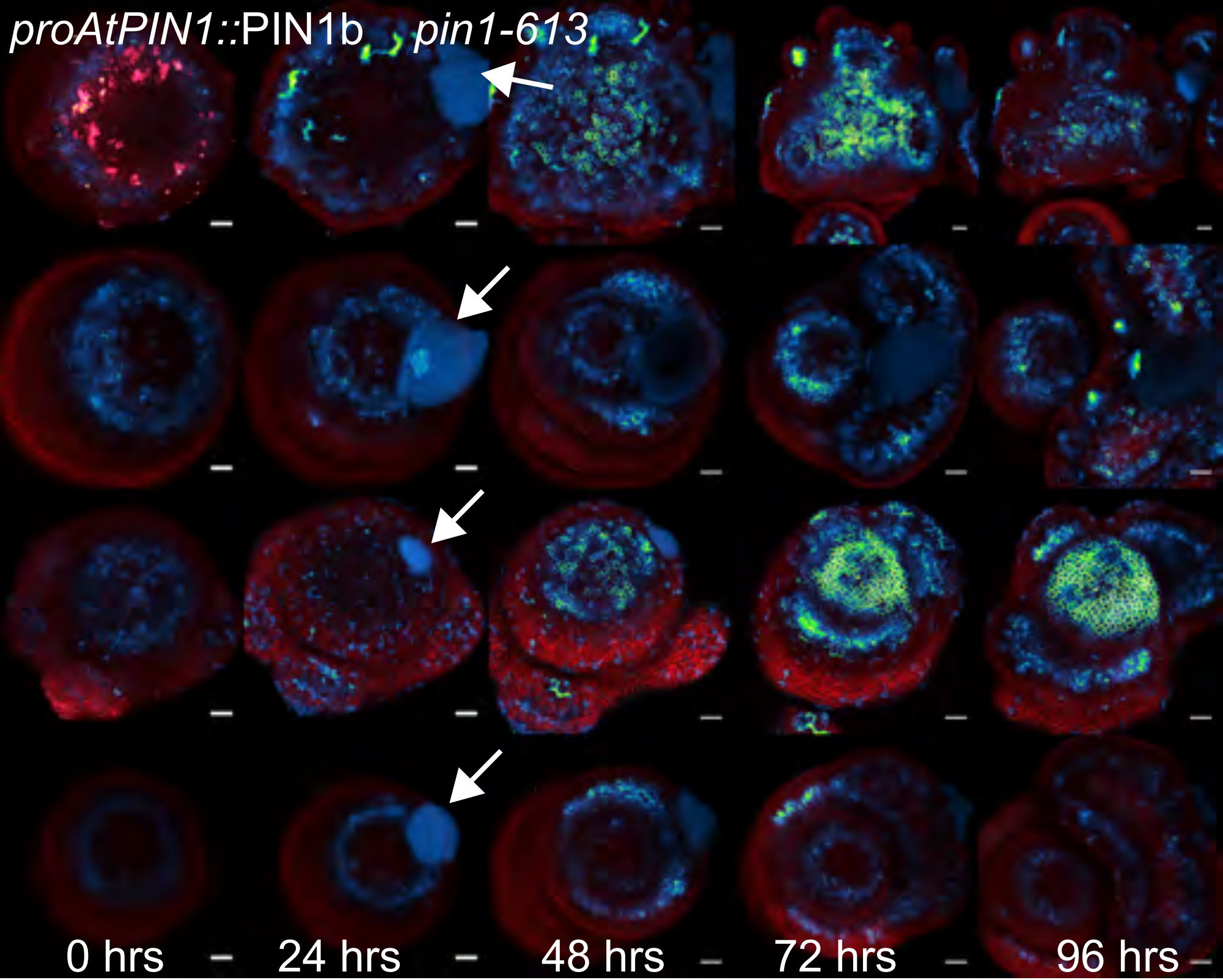

Figure 5 - supplement 3

Figure 6. SoPIN1 and PIN1b show different behaviors under *proAtML1*-driven expression. Maximum projections of *proAtML1::*LhG4 driving pOP::SoPIN1 or pOP::PIN1b (*proAtML1*>>SoPIN1 and *proAtML1*>>PIN1b) in wild-type Landsberg *erecta* (L*er)* **(A-D),** and *pin1-4* **(E-L)** inflorescence meristems and basal internodes. **(A)** SoPIN1 and **(B)** PIN1b maximum projections of wild-type L*er* inflorescence meristems. I3, I2, I1, and P1 primordia are indicated. White boxes around each I2 primordium indicate the regions detailed in **(C-D).** Asterisk in **(C)** indicates convergence point. Arrow in **(D)** indicates punctate PIN1b. **(E)** SoPIN1 and **(F)** PIN1b maximum projections of complemented *pin1-4* meristems. I3, I2, I1, and P1 primordia are indicated. White boxes around each I2 primordia indicate the regions detailed in **(G-H)**. Asterisks mark convergence points in **(G)** and **(H)**. Red signal in **(C,D,G,H)** is cell wall propidium iodide staining. See Figure 6 – supplement 1 for additional samples of *proAtML1*>>SoPIN1 and Figure 6 – supplement 2 for additional samples of *proAtML1*>>PIN1b in both WT and *pin1-4* meristems. See Figure 6 - supplement 3 for details of PIN1b epidermal intracellular localization in WT and *pin1-4* meristem apexes. **(I-J)** Tiled maximum projections of cross hand-sections of the basal internode of SoPIN1 **(I)** and PIN1b **(J)** -complemented *pin1-4* plants showing PIN signal in the outer cortex layers (arrows). Red signal in **(I-J)** is chlorophyll auto-florescence. **(K-L)** Epidermal maximum projections showing rootward polarized PIN localization (arrows) in the basal internode of SoPIN1 **(K),** and PIN1b **(L)** -complemented *pin1-4* plants. Scale bars: 25µm in **(A-H)**. 100µm in **(I-L)**.

Figure 6 – supplement 1. *proAtML1*>>SoPIN1 representative meristem maximum projections. (A) *proAtML1*>>SoPIN1 expression in three different wild-type L*er* meristems. **(B)** *proAtML1*>>SoPIN1 expression in three different complemented *pin1-4* meristems. Capture settings are identical in all samples. Scale bars: 25µm.

Figure 6 – supplement 2. *proAtML1*>>PIN1b representative meristem maximum projections. (A) *proAtML1*>>PIN1b expression in three different wild-type L*er* meristems. **(B)** *proAtML1*>>PIN1b expression in three different complemented *pin1-4* meristems. Capture settings are identical in all samples. Scale bars: 25µm.

Figure 6 – supplement 3. Subcellular localization of PIN1b in wild-type (L*er*) and *pin1-4* meristems. (A) Wild-type (L*er*) meristem expressing *proAtML1*>>PIN1b. Boxes numbered 1-3 indicate the positions of detail images in **(B-D). (B)** Organ boundary. **(C)** Incipient organ. **(D)** Meristem apex. **(E)** *pin1-4* meristem complemented by *proAtML1*>>PIN1b. Boxes numbered 1-3 indicate the positions of detail images in (**F-H).** **(F)** Meristem apex. **(G)** Organ boundary. **(H)** Convergence point, indicated by asterisk. Red signal is FM4-64 vital stain. Scale bars: 5µm.

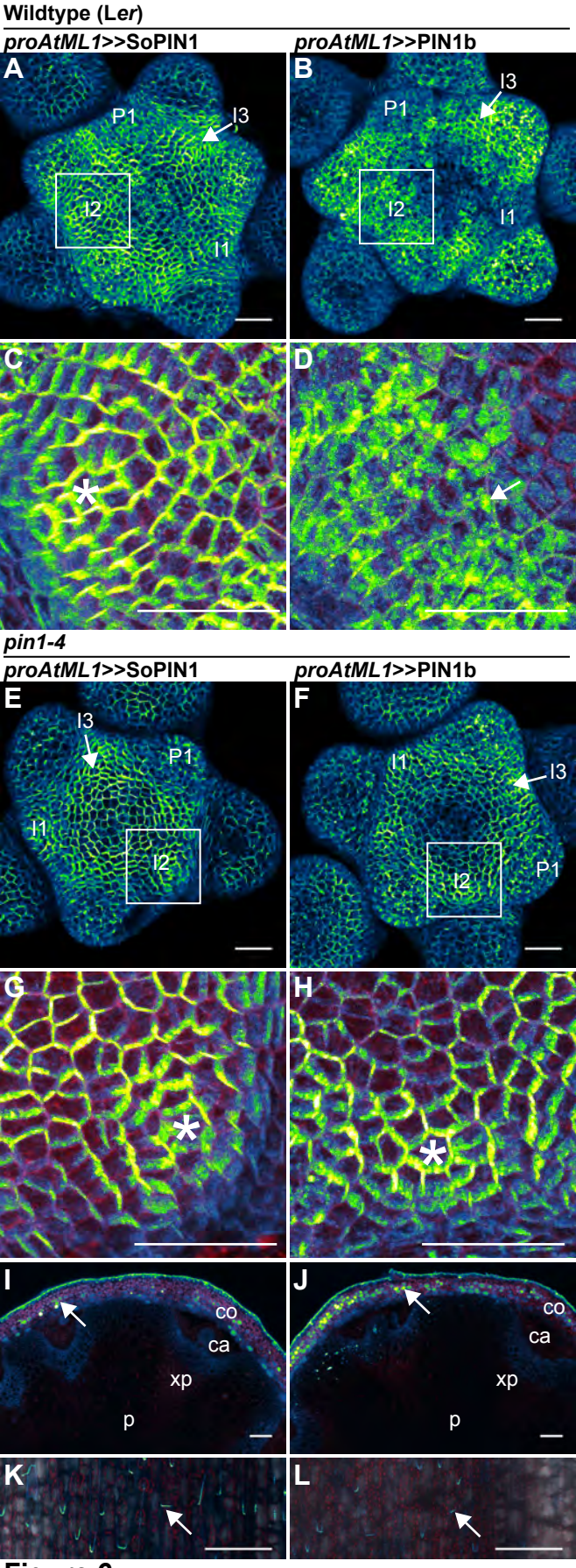
Wildtype (Ler)
proAtML1>>SoPIN1
proAtML1>>PIN1b
A
P1
I3
I2
I1
B
P1
I3
I2
I1
C
D
pin1-4
proAtML1>>SoPIN1
proAtML1>>PIN1b
E
I3
P1
I1
I2
F
I1
I3
I2
P1
G
H
I
co
ca
xp
p
J
co
ca
xp
p
K
L

Figure 6

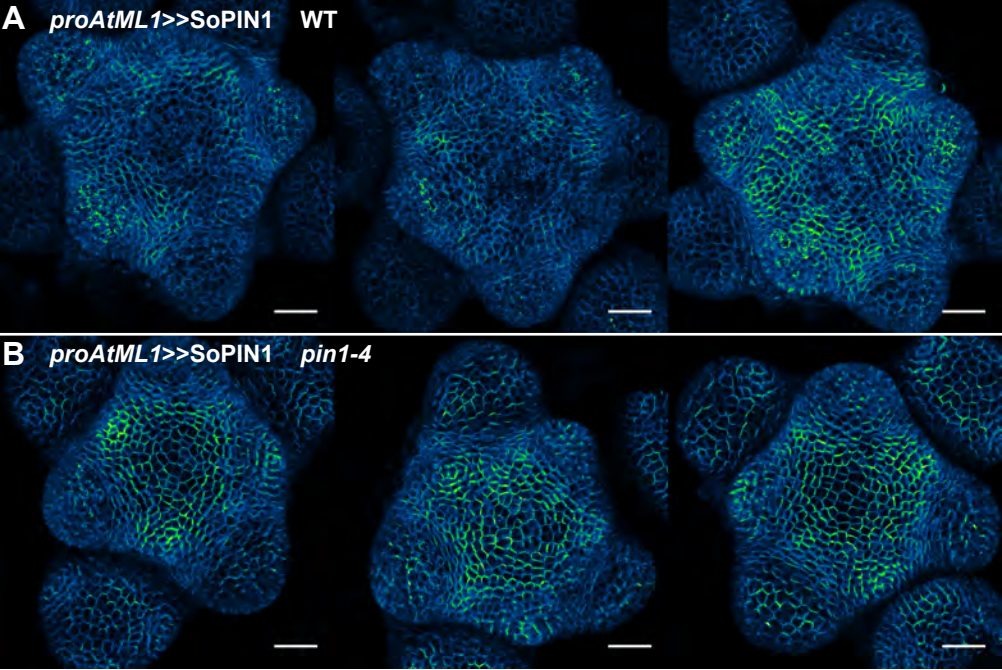

Figure 6 - supplement 1 - *proAtML1*>>SoPIN1

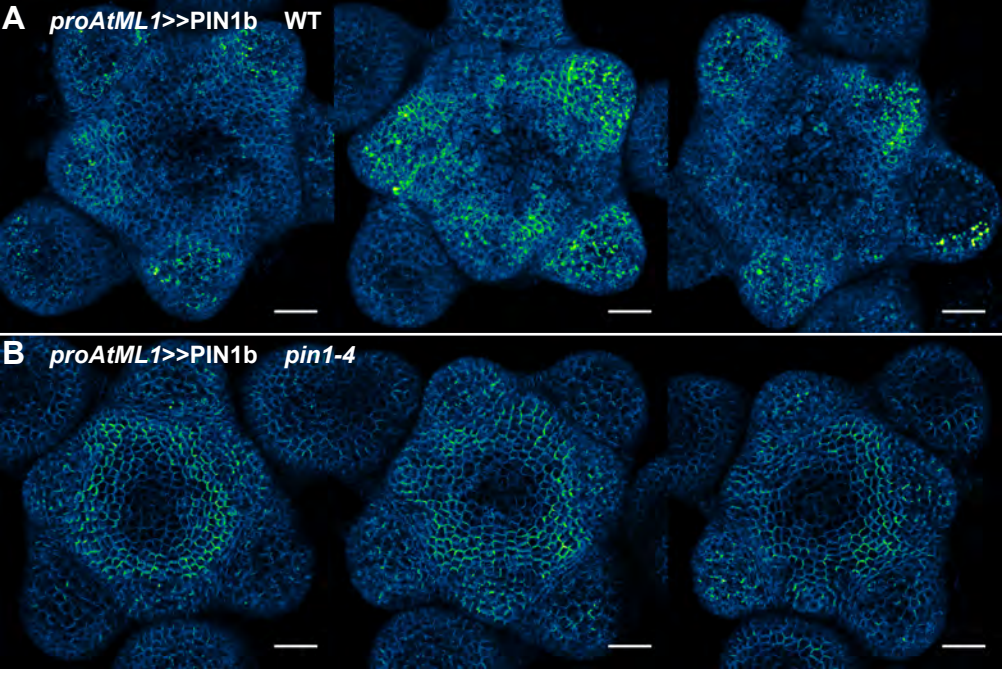

Figure 6 - supplement 2 - *proAtML1*>>PIN1b

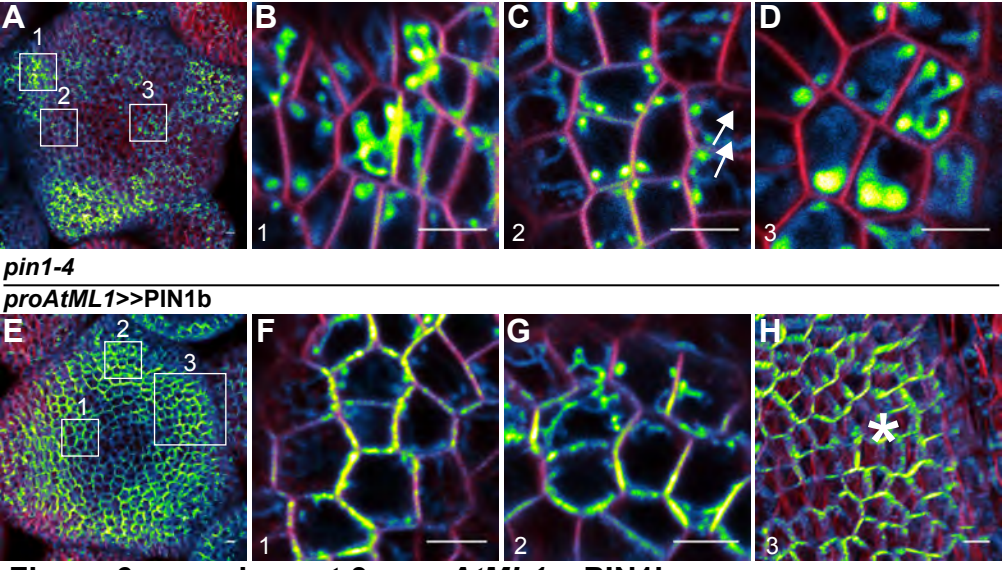

Figure 6 - supplement 3 - *proAtML1*>>PIN1b

Figure 7. AtPIN1 protein immuno-localization in wild-type, *pin1-613,* and *pin1-4* meristems. (A) AtPIN1 protein accumulation in wild-type L*er* inflorescence apex shows polar PIN protein at the sites of initiating organs (asterisk), and during vein patterning below the apex (arrow). **(B)** No AtPIN1 protein is detected in *pin1-613* null mutant pin-formed apexes. **(C)** Abundant AtPIN1 protein is detected in *pin1-4* pin-formed apexes, primarily in provascular tissues below the meristem apex (arrow). Box shows region of detail in **(D). (D)** Detail of boxed area shown in **(C)**. AtPIN1 protein in *pin1-4* accumulates in a perinuclear domain (arrow). All samples are 9µm longitudinal sections. Scale bars: 25µm in A-C, and 5µm in D.

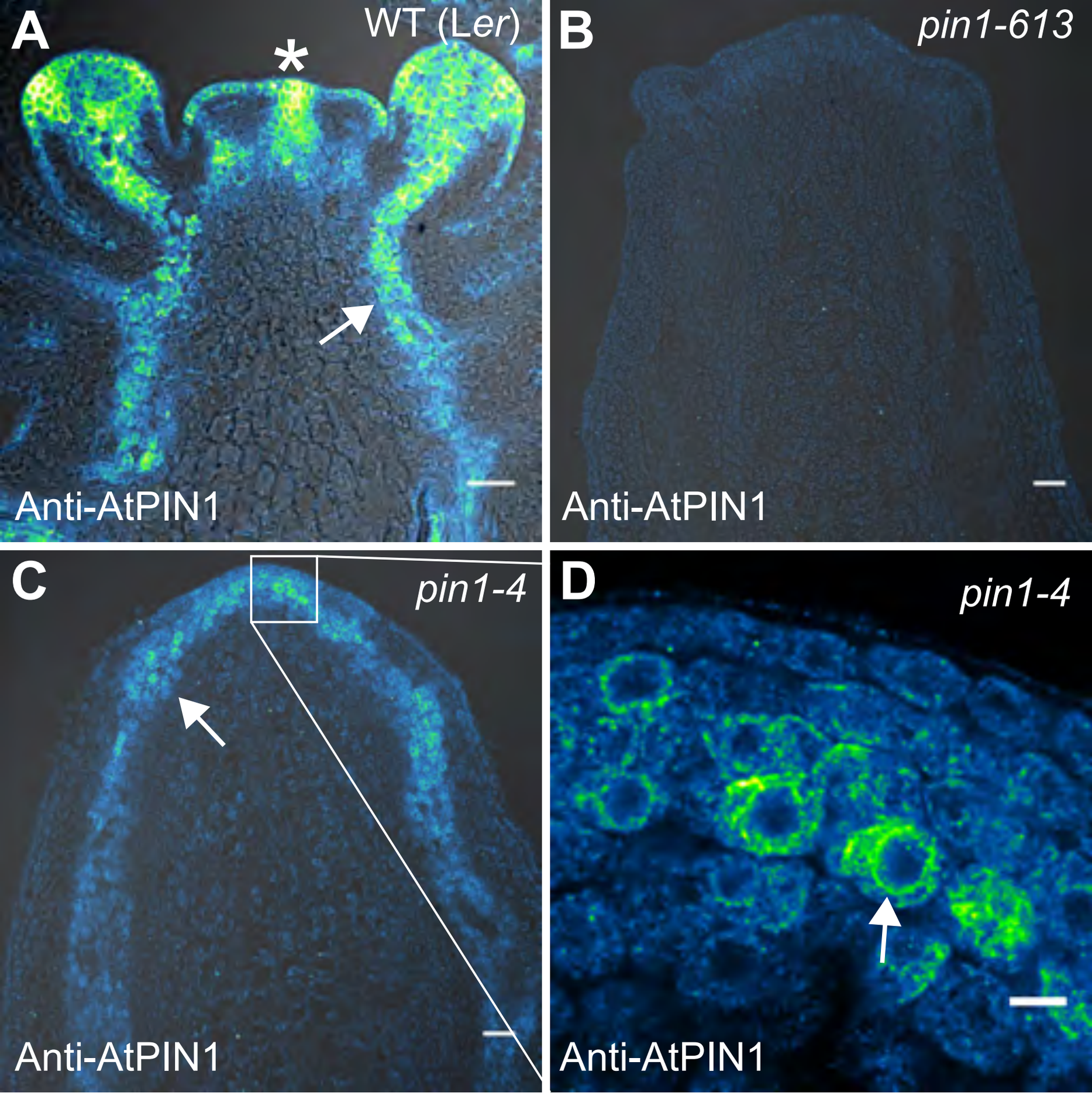
A
WT (Ler)
*
Anti-AtPIN1
B
pin1-613
Anti-AtPIN1
C
pin1-4
Anti-AtPIN1
D
pin1-4
Anti-AtPIN1

Figure 7

Figure 8. Both SoPIN1 and PIN1b can complement Arabidopsis *pin1-4* under *proAtML1*-driven expression. (A) From left to right, wild-type L*er, proAtML1*>>PIN1b complemented *pin1-4, proAtML1*>>SoPIN1 complemented *pin1-4, and pin1-4 alone.* Arrow indicates barren pin inflorescence in *pin1-4*. See Figure 8 – supplement 1 for inflorescence phenotypes. **(B)** Box-plot of bulk auxin transport (counts per minute, CPM) through basal internodes 1cm above the rosette of 40-day-old Arabidopsis inflorescence stems (n=16 each genotype). Samples with different letters are significantly different from each other (ANOVA, Tukey HSD, $p < 0.05$). See Figure 8 - Source Data 1 for source data. **(C)** Box-plot of stem cross-sectional area (square mm) of the basal internode 1cm above the rosette (n=12 each genotype). Samples with different letters are significantly different from each other. (ANOVA, Tukey HSD, $p < 0.05$). See Figure 8 - Source Data 2 for source data. Representative Toluidine Blue O stained hand cross-sections are shown above each box for each genotype. Scale bars: 1cm in **(A)**. 500µm in **(C).**

Figure 8 – supplement 1. *proAtML1*>>SoPIN1 and *proAtML1*>>PIN1b complemented *pin1-4* inflorescence phenotypes. (A) Wild-type L*er*, **(B)** *proAtML1*>>SoPIN1 complemented *pin1-4,* and **(C)** *proAtML1*>>PIN1b complemented *pin1-4* inflorescence apexes. Scale bars: 1mm.

Figure 8 - Source Data 1. Source data for Figure 8B auxin transport assays.

Figure 8 - Source Data 2. Source data for Figure 8C stem cross-sectional area measurements.

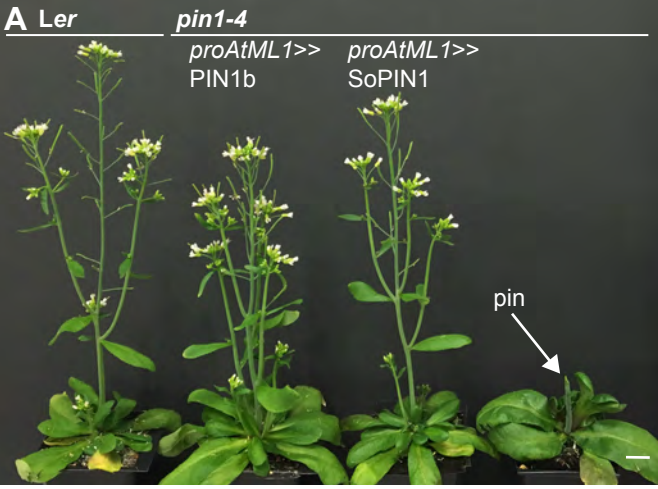
A Ler
pin1-4
proAtML1>>
PIN1b
proAtML1>>
SoPIN1
pin

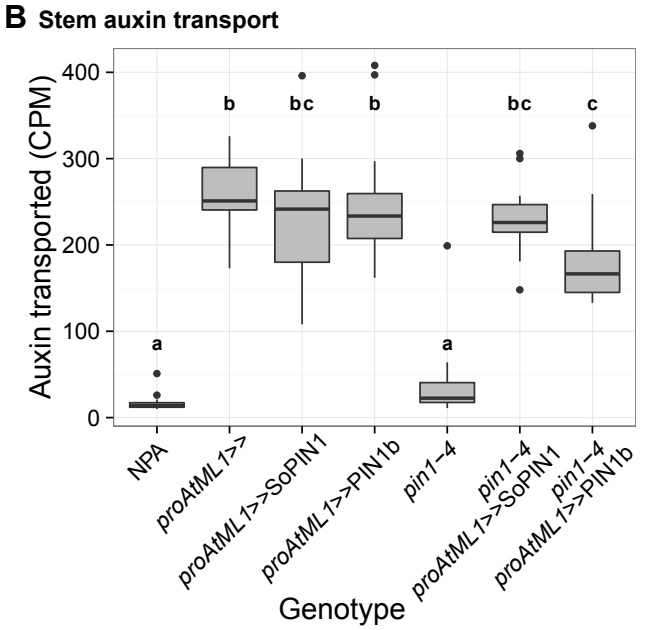
B Stem auxin transport
Auxin transported (CPM)
400
300
200
100
0
a
b
bc
b
a
bc
c
NPA
proAtML1>>
proAtML1>>SoPIN1
proAtML1>>PIN1b
pin1−4
pin1−4 proAtML1>>SoPIN1
pin1−4 proAtML1>>PIN1b
Genotype

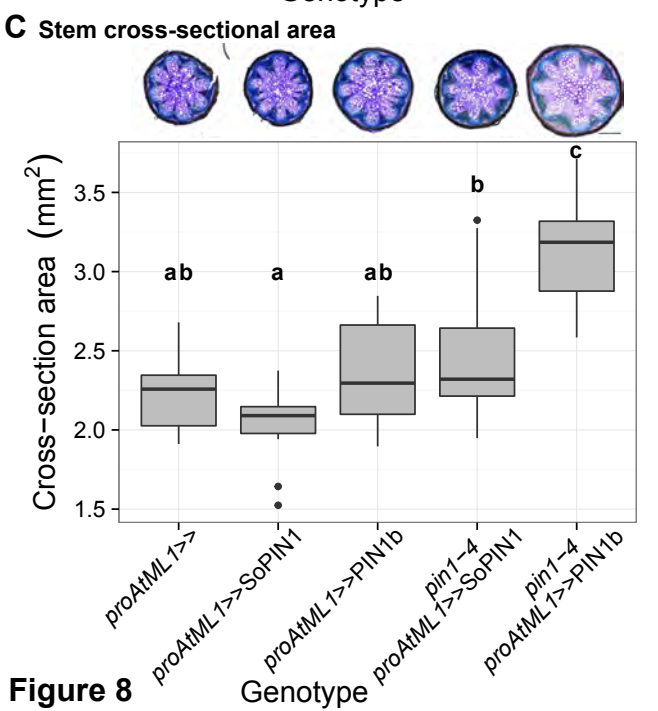
C Stem cross-sectional area
Cross−section area (mm2)
3.5
3.0
2.5
2.0
1.5
ab
a
ab
b
c
proAtML1>>
proAtML1>>SoPIN1
proAtML1>>PIN1b
pin1−4
pin1−4 proAtML1>>SoPIN1
pin1−4 proAtML1>>PIN1b
Genotype

Figure 8

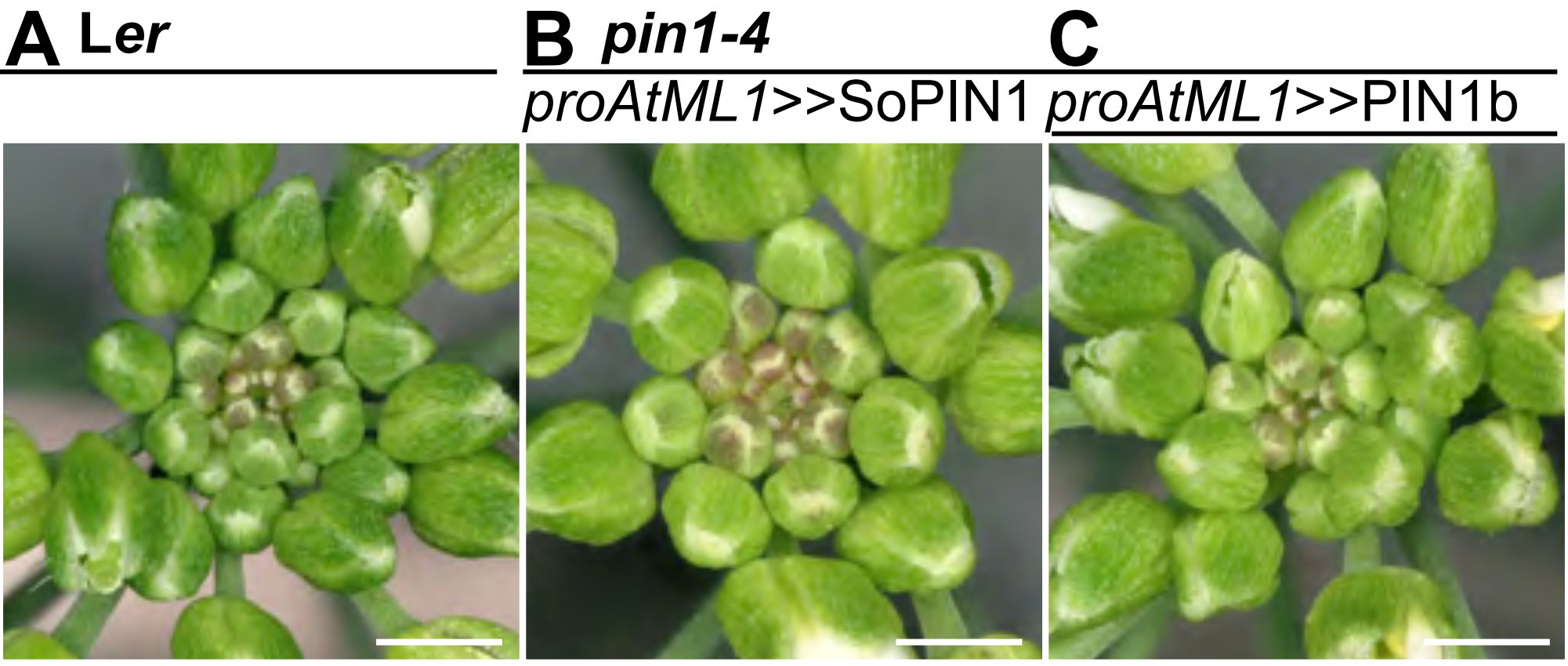

Figure 8 - supplement 1

Figure 9. Heterologous expression visual summary: Functional distinction between PIN auxin efflux proteins during development. Polarized SoPIN1 is represented by green lines, polarized PIN1b by blue lines, un-polarized PIN1b by blue circles, and the putative partially functional *pin1-4* protein is indicated by magenta circles. Red arrows indicate measured auxin transport in the basal internode, while red bar-headed lines indicated reduced transport. Black arrows represent polarized PIN patterns. Convergence points are marked with asterisks. **(A)** When expressed in both the epidermis and internal tissues with *proAtPIN1* in wild-type Col-0, SoPIN1 forms convergent polarization patterns in the epidermis and is partially able to rescue the organ initiation phenotypes and bulk transport in null *pin1-613* mutants. **(B)** When SoPIN1 is expressed only in the epidermis from the *proAtML1* promoter, it forms convergence points in the wild-type background and is able to rescue more fully the organ initiation phenotypes of the *pin1-4* single amino acid change mutation in L*er.* **(C)** In contrast, when PIN1b is expressed in both the epidermis and internal tissues from the *proAtPIN1* promoter in wild-type Col-0, it accumulates mostly in the internal tissues, and is unable to complement the *pin1-613* organ initiation phenotype. It is also unable to transport auxin through stem segments, despite apparently AtPIN1-like accumulation and polarization in the stem. **(D)** When PIN1b is expressed in the epidermis from the *proAtML1* promoter it does not form convergent polarization patterns and is often un-polarized in the wild-type *Ler* background (blue ovals), but it does in the *pin1-4* background, where it is able to rescue the defective organ initiation phenotype and mediate bulk transport. See Figure 9 - supplement 1 for a protein alignment comparing AtPIN1 to other PIN1-clade protein sequences from diverse angiosperms.

Figure 9 - supplement 1. Brassicaceae-specific PIN1 domains. (A) Wrapped protein alignment showing PIN1 clade members from across the angiosperms. Grass PIN1a proteins are indicated with grey rectangle, grass PIN1b proteins are indicated with black rectangle, and Brassicaceae PIN1 proteins are indicated with red rectangle. Domains that are unique to the Brassicaceae family proteins are indicated by transparent red boxes over the alignment. **(B)** Sequenced angiosperm species and version numbers, from https://phytozome.jgi.doe.gov. Species used in the alignment in **(A)** are indicated with green circles. See Figure 9 - Source Data 1 for source data.

Figure 9 - Source Data 1. FASTA alignment source data for Figure 9 - supplement 1.

Table 1. Primers. See methods for usage.

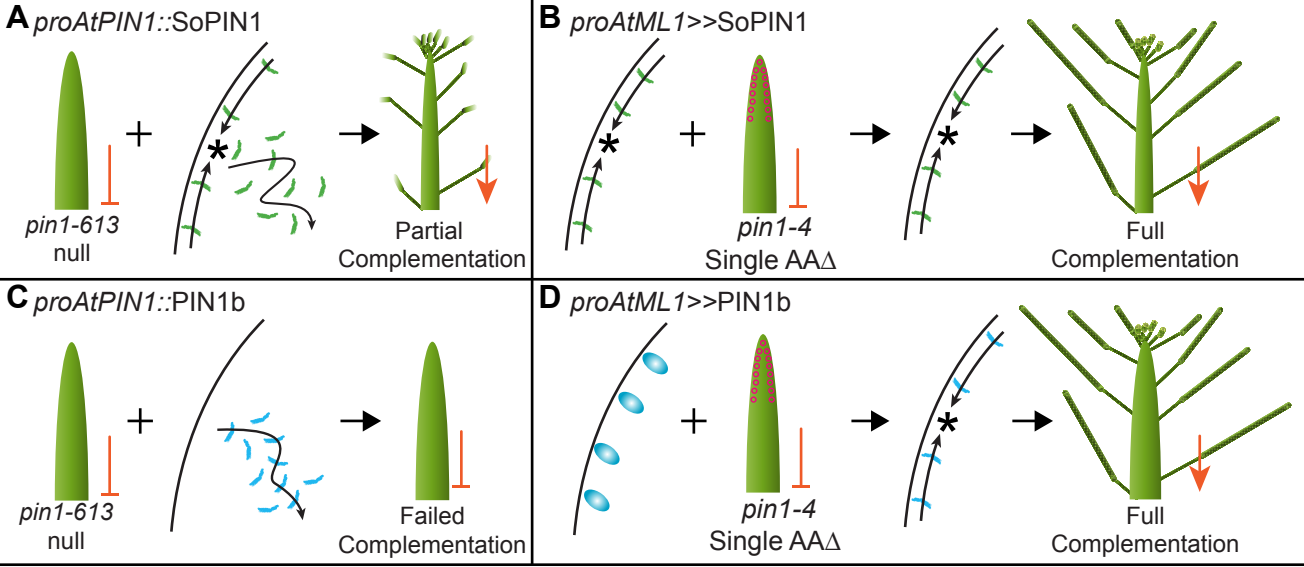
A proAtPIN1::SoPIN1
pin1-613
null
Partial
Complementation
B proAtML1>>SoPIN1
pin1-4
Single AAΔ
Full
Complementation
C proAtPIN1::PIN1b
pin1-613
null
Failed
Complementation
D proAtML1>>PIN1b
pin1-4
Single AAΔ
Full
Complementation
SoPIN1
PIN1b
Apolar PIN1b
pin1-4
Polarity
Convergence Point
Transport
Reduced

Figure 9

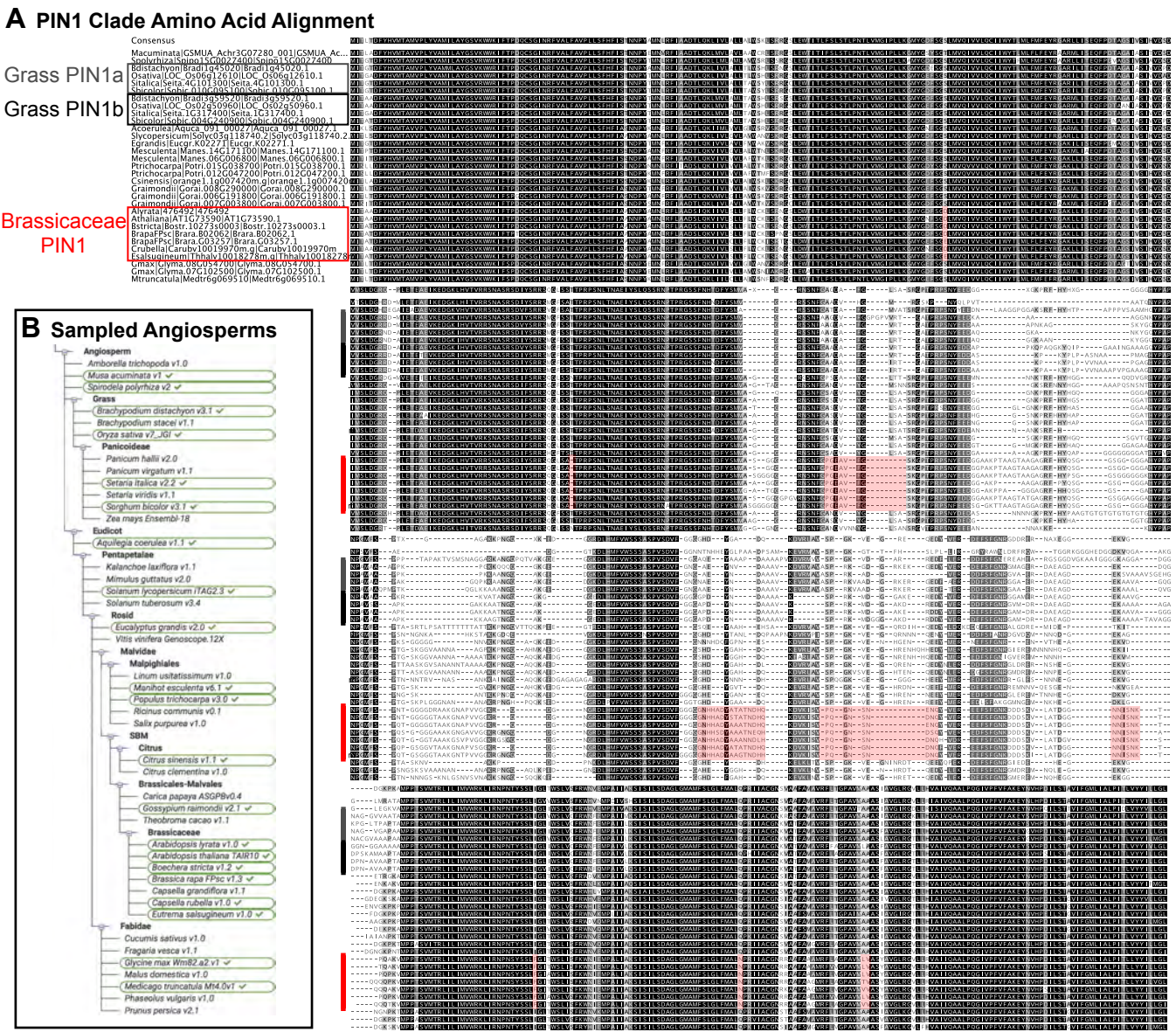

Figure 9 - supplement 1

Table 1: Primers

ID#	Name	Sequence	Purpose
1	524_Bradi4g26300_4230_F	CGTTCCGTGTTGATTCCGATG	*sopin1-1* genotyping with HgaI digestion
2	525_Bradi4g26300_4923_R	CTGGAGTAGGTGTTGGGGTTC	*sopin1-1* genotyping with HgaI digestion
3	526_Cas9_8622_F	TCCCAGAGAAGTACAAGGAGATCT	Cas9 Genotyping
4	527_Cas9_9159_R	TTGTACACGGTGAAGTACTCGTAG	Cas9 Genotyping
5	104_BdPIN_11_QPCR_F	ACAACCCTTACGCCATGAAC	*pin1a-1* genotyping with NcoI digestion
6	473_PIN1a_dom1_shortR	CACACGAACATGTGCAGGTC	*pin1a-1* genotyping with NcoI digestion
7	541_Bradi3g59520_PIN1b_5084_F	TGATGCTCTTCATGTTCGAGTACC	*pin1b-1* genotyping with mboI digestion
8	542_Bradi3g59520_PIN1b_5838_R	GGAGTAAACTACGTTGTGACAAGG	*pin1b-1* genotyping with mboI digestion
9	019 - Ubi-1 Prom attB4 F	GGGGACAACTTTGTATAGAAAAGTTGCTGCAGTGCAGCGTGACCCGG	pZmUbi amplification for cloning
10	020 - Ubi-1 Prom attB1 R	GGGGACTGCTTTTTTGTACAAACTTGCTGCAGAAGTAACACCAAACA	pZmUbi amplification for cloning
11	PIN1pro-GW-F	GGGGACAACTTTGTATAGAAAAGTTGTTACCCTCATCCATCATTAACTT	*proAtPIN1* amplification
12	PIN1pro-GW-R	GGGGACTGCTTTTTTGTACAAACTTGTCTTTTGTTCGCCGGAGAAGAGA	*proAtPIN1* amplification
13	455 BdSoPIN1 cacc mRNA	TCACATCTGCTGCCGCTGCC	SoPIN1-Citrine coding region amplification
14	302 - PIN_7 qPCR UTR R2	AATCCCAAAAGCCGACATTG	SoPIN1-Citrine coding region amplification
15	466 BdPIN1b cacc mRNA-2	CACCTGTACACACTGCGGCGCT	PIN1b-Citrine coding region amplification
16	308 - PIN_5 qPCR UTR R1	ACTCGCTAACCAACCCCTTAATT	PIN1b-Citrine coding region amplification
17	MVR087 - pin1-613 RP (SALK_047613)	AATCATCACAGCCACTGATCC	*pin1-613* genotyping
18	MVR086 - pin1-613 LP (SALK_047613)	CAAAAACACCCCCAAAATTTC	*pin1-613* genotyping
19	MVR036 - LBb1.3	ATTTTGCCGATTTCGGAAC	*pin1-613* genotyping
20	344 - Citrine Seq R	GAAGCACATCAGGCCGTAG	PIN1b-Citrine and SoPIN1-Citrine genotyping
21	524_Bradi4g26300_4230_F	CGTTCCGTGTTGATTCCGATG	SoPIN1-Citrine genotyping
22	541_Bradi3g59520_PIN1b_5084_F	TGATGCTCTTCATGTTCGAGTACC	PIN1b-Citrine genotyping
23	543_pin1-4_Aci_F	GCTTTTGCGGCGGCTATGAGATTTGT	*pin1-4* genotyping with AciI digestion
24	544_pin1-4_Aci_R	GCTTCTGATTTAATTTGTGGGTTTTCA	*pin1-4* genotyping with AciI digestion
25	076 - BASTA_F2	CTTCAGCAGGTGGGTGTAGAG	ML1::LhG4 genotyping
26	077 - BASTA_R2	GAGACAAGCACGGTCAACTTC	ML1::LhG4 genotyping